

Link Scheduling using Graph Neural Networks

Zhongyuan Zhao, Gunjan Verma, Chirag Rao, Ananthram Swami, and Santiago Segarra

Abstract—Efficient scheduling of transmissions is a key problem in wireless networks. The main challenge stems from the fact that optimal link scheduling involves solving a maximum weighted independent set (MWIS) problem, which is known to be NP-hard. For practical link scheduling schemes, centralized and distributed greedy heuristics are commonly used to approximate the solution to the MWIS problem. However, these greedy schemes mostly ignore important topological information of the wireless network. To overcome this limitation, we propose fast heuristics based on graph convolutional networks (GCNs) that can be implemented in centralized and distributed manners. Our centralized MWIS solver is based on tree search guided by a trainable GCN module and 1-step rollout. In our distributed MWIS solver, a trainable GCN module learns topology-aware node embeddings that are combined with the network weights before calling a distributed greedy solver. Test results on medium-sized wireless networks show that a GCN-based centralized MWIS solver can reach a near-optimal solution quickly. Moreover, we demonstrate that a shallow GCN-based distributed MWIS scheduler can reduce by nearly half the suboptimality gap of the distributed greedy solver with minimal increase in complexity. The proposed scheduling solutions also exhibit good generalizability across graph and weight distributions.

Index Terms—Maximum weighted independent set, graph convolutional network, wireless network, scheduling.

I. INTRODUCTION

A fundamental problem in managing wireless networks is to efficiently schedule transmissions. In general, the scheduling problem involves determining which links should transmit and when they should transmit, along with other relevant parameters such as transmit power, modulation, and coding schemes [2]–[4]. In this paper, we focus on link scheduling in wireless networks with time-slotted orthogonal multiple access, in which a time slot comprises a scheduling phase followed by a transmission phase [5], [6]. This problem is associated with many real-world applications of both ad-hoc and infrastructure-based wireless networks, e.g., battlefield communications, vehicular/flying ad-hoc networks, wireless sensor networks [7], [8], device-to-device (D2D) communications [9], cloud-radio access networks (CRAN) [10], wireless backhaul networks [5], [11], multi-hop relay networks for

Z. Zhao and S. Segarra are with the Department of Electrical and Computer Engineering, Rice University, USA. e-mails: {zhongyuan.zhao, segarra}@rice.edu

G. Verma, C. Rao, and A. Swami are with the US Army’s DEVCOM Army Research Laboratory, USA. e-mails: {gunjan.verma.civ, chirag.r.rao.civ, ananthram.swami.civ}@mail.mil.

Research was sponsored by the Army Research Office and was accomplished under Cooperative Agreement Number W911NF-19-2-0269. The views and conclusions contained in this document are those of the authors and should not be interpreted as representing the official policies, either expressed or implied, of the Army Research Office or the U.S. Government. The U.S. Government is authorized to reproduce and distribute reprints for Government purposes notwithstanding any copyright notation herein.

Preliminary results were presented in [1].

mmWave and THz bands communications [12], [13], and internet of things [14], [15]. Compared to contention-based multiple access, e.g. CSMA-CA, scheduled multiple access is often preferred due to its increased spectrum utilization efficiency [16]. This benefit, however, comes with the associated challenge that optimal scheduling involves solving a maximum weighted independent set (MWIS) problem [2]–[6], [10], [17]–[22], which is NP-hard [22], [23]. The idea of scheduling links by selecting the MWIS of the conflict graph of a network was first established in [2], and has been developed since then [3]–[6], [10], [17]–[22]. Such link scheduling schemes involve two major tasks: 1) A per-link utility function to compute the weights associated with activating each link, and 2) An efficient (possibly distributed) *MaxWeight* [2], [18] scheduler as an approximate solver for the associated MWIS problem.

In terms of the per-link utility design, queue length [2], [3], [17], link rate [10], their product [18] and ratio [6], and the age of information [24] have been used in the past, along with some more theoretically-grounded variations [4]. Moreover, routing decisions can be involved in the per-link utility. In backpressure routing [2], [25], the per-link utility for scheduling is the queue length of a flow decided by a routing algorithm for throughput-optimal routing [2] or a virtual queue length for delay-optimal routing [25]. Utility functions can promote not only traffic metrics, but also fairness across the network [26]. Besides analytical functions, the per-link utilities can also be generated by a reinforcement learning (RL) agent with a continuous action space [11], where the transition of network state is modeled as a Markov decision process.

For MaxWeight scheduling, a good MWIS solver is defined by high quality and low complexity, and should be agnostic to the choice of the per-link utility function. The quality of a solution is measured by its approximation ratio (AR) to the optimal solution. Further, low communication and computational complexity can reduce scheduling overhead. Many heuristics have been developed for lower complexity and/or better performance [3], [6], [10], [17]–[21], [27]. Centralized MWIS solvers, with limited scalability but high AR provided by the global information of the network, can be used as schedulers for infrastructure-based networks [5], [9]–[11], and for theoretical exploration of network capacity [4]. On the other hand, distributed MWIS solvers are preferred for practical scheduling in wireless ad-hoc networks since they can reduce the computational overhead through parallelism, and eliminate the need for relaying packets over the network by limiting communications to local neighborhoods. Moreover, distributed scheduling increases network robustness against a single point of failure at the fusion center. Without global information, distributed MWIS solvers seek to achieve reasonable performance efficiently, e.g., with linear [6], [10], [19], [20], logarithmic [3], [17], [18], or constant [17], [21], [27]

local communication complexity (referred to as *local complexity*), which is defined as the required rounds of information exchange in the neighborhood (referred to as *local exchange*). As the common choice of practical scheduling schemes, the category of distributed greedy heuristics [3], [17], [18] seeks to mimic an iterative process of adding the link with the largest utility to the partial solution and removing other links that might interfere with it.

Motivated by the success of machine learning in other fields, data-driven learning-based solutions for resource allocation problems in wireless networks have been proposed over the last few years [28]–[34]. A common practice in most of these approaches is to parameterize a function of interest using multi-layer perceptrons (MLP) or convolutional neural networks (CNNs), which are not well-suited for problems in wireless communications since they do not exploit the underlying topology. This has led to several approaches that tried to adjust CNNs to the wireless setting [28], [35]–[37]. Here, we adopt an alternative direction [33], [38], in which graph neural networks (GNNs) [39]–[42] are used to incorporate the topology of the wireless network into the learning algorithm.

Our approach is also in line with the recent trend of using deep learning to find approximate solutions to combinatorial problems on graphs [43], [44]. More precisely, we propose a fast centralized MWIS solver and a low-complexity distributed solver based on graph convolutional networks (GCNs) [45]–[47]. Our *centralized* MWIS solver adopts a 1-step rollout search in the GCN-guided tree search [44] to ensure that the first leaf reached is of high quality, thus reducing the complexity by several orders of magnitude. On the other hand, our *distributed* MWIS solver has a novel modular structure where a GCN-based node embedding module is followed by a distributed greedy heuristic, thus exploiting the efficiency of the latter while raising graph-awareness through the use of the GCN. Moreover, the GCN can be trained in an unsupervised manner – i.e., without the need to exactly solve any MWIS problem – and, although the training must be centralized, the deployment is fully distributed.

Contributions: We develop efficient approximate MWIS solvers suitable for link scheduling in wireless networks. Specifically: 1) We propose the first GCN-based distributed MWIS solver for link scheduling by combining the topology-awareness of GCNs and the efficiency of distributed greedy solvers; 2) We propose fast centralized MWIS solvers based on a GCN-guided tree search that can achieve near optimal performance on medium-sized graphs with hundreds of nodes; 3) We develop a reinforcement learning scheme to train the GCNs with the help of efficient heuristics, which has better performance and computational efficiency than alternative supervised learning schemes; and 4) Through numerical experiments, we demonstrate the superior performance of the proposed method in single and multi-channel scheduling as well as its generalizability over different graph types and weight distributions.

Paper outline: The rest of this paper is organized as follows. Related work is reviewed in Section II. The system model and the formulation of the scheduling problem are introduced in Section III. The proposed GCN-based *central-*

ized MWIS solver is described in Section IV, followed by our GCN-based *distributed* MWIS solver in Section V. In Section VI, numerical experiments illustrate the performance of our proposed solutions in comparison with current state-of-the-art methods. Section VII wraps up the paper with a short conclusion and a discussion on future directions.

Notation: Upright bold lower-case symbols (e.g., \mathbf{x}) are used to denote column vectors, whereas upright bold upper-case symbols (e.g., \mathbf{X}) are used to represent matrices. Calligraphic upper-case symbols (e.g., \mathcal{V}) are used to denote sets, whereas the corresponding bold lower-case symbols (e.g., \mathbf{v}) represent subsets. A graph \mathcal{G} is defined by a set $\mathcal{V} = \{1, \dots, V\}$ of vertices and a set \mathcal{E} of edges, where $V = |\mathcal{V}|$ by convention, and $(i, j) \in \mathcal{E}$ indicates that there exists an (undirected) edge between vertices i and j . The set of neighbors of a vertex $v \in \mathcal{V}$ is denoted by $\mathcal{N}(v)$. To avoid confusion, we refer to a node in a wireless network as *user*, a node in a conflict graph as *vertex*, and a node in other graphs, such as a search tree, as *node*.

II. RELATED WORK

The MWIS problem has been studied for decades. Centralized solvers based on exact, heuristic, and hybrid algorithms have been developed [48]–[53]. To find the exact solution, the MWIS problem can be formulated following integer programming, maximum satisfiability, or graph coloring approaches, and solved via mixed integer programming solvers [54] based on branch-and-bound schemes [48]–[50]. For general graphs, exact solvers only work on medium-sized graphs of up to hundreds of vertices, since the MWIS problem is NP-hard. For real-world graphs, however, their structural properties can be utilized to improve the efficiency of exact solvers [5], [53]. For networks with a tree topology, the MWIS problem can be solved efficiently [5]. Moreover, a full suite of rule-based graph reduction techniques has been developed to exploit the hierarchical structure of large real-world graphs [53], which can drastically reduce the effective size of graphs being processed in iterative frameworks and allow the exact solvers to work for some real-word graphs of up to millions of vertices. For medium to large-sized graphs that are unsolvable by the exact solvers, heuristics based on local search can often obtain approximate solutions with high quality [55]–[58]. In addition, quantum approximate optimization combining quantum and classical computing has been recently proposed for heuristic solvers [27], [59]. Nonetheless, the aforementioned centralized MWIS solvers are not suitable for link scheduling due to complexity [5], since centralized link scheduling generally requires solving the MWIS problem on small graphs within milliseconds. Our centralized MWIS solver is specifically designed to work on general graphs at low complexity in terms of time and communication.

For practical scheduling in wireless ad-hoc networks, distributed MWIS solvers with low communication and computational complexity are usually preferred. Distributed MWIS solvers [6], [10], [19]–[21], [27], [60] construct a solution through an iterative procedure of a round of local exchanges between a vertex and its neighbors, followed by a phase of processing on each vertex. Thus, it is best to describe the

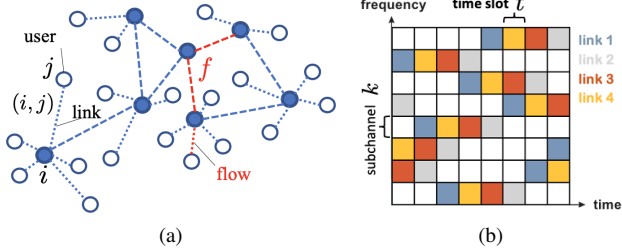


Fig. 1: Wireless multi-hop network with orthogonal access. (a) Connectivity graph of the network. (b) Example of orthogonal access in an FDMA system, where the spectrum is divided into sub-channels, time is divided into time slots, and each spectral-temporal slot can be accessed by at most one link in a set of potentially interfering links.

complexity of distributed MWIS solvers with *local (communication) complexity*, defined as the number of rounds of local exchanges between each vertex and its neighbors. In [6], [10], [19], a solution is obtained in 2 steps, each with a linear local complexity of $\mathcal{O}(V)$: first, solve the linear relaxation of the integer programming formulation of the MWIS problem with clique constraints, then the solution of step 1 is used as initial weights to estimate the solution in a distributed manner. In [20], a solution is constructed through $\mathcal{O}(V)$ iterations of combining feasible local solutions at each vertex and exchanging the results with its neighbors. Compared with distributed solvers with linear local complexity $\mathcal{O}(V)$ [6], [10], [19], [20], Ising-formulated MWIS solvers [21], [27], [60] require a fixed number of rounds (e.g. tens to hundreds) of local exchanges to emulate the cooling process of atoms with magnetic spin. The distributed greedy solvers [17], [18] have an average local complexity of $\mathcal{O}(\log V)$, and the worst-case local complexity of $\mathcal{O}(V)$ on certain graphs. In particular, the local greedy solver (LGS) [17] selects vertices with the largest weights among their neighbors with a built-in tie resolution mechanism, and then excludes the neighbors of the selected vertices. Randomization is introduced in [18] to improve the performance of LGS, which is deterministic; a vertex is selected if its weight exceeds a prescribed fraction of the maximal weight of its neighbors. Our distributed MWIS solver departs from existing work by incorporating topological information in the solution through a trainable node embedding procedure.

GNNs have been recently proposed to approximate the solution to combinatorial problems [43], [61] including the maximal (unweighted) independent set (MIS) problem [44], the Boolean satisfiability problem [62], the traveling salesman problem [63], and maximum constraint satisfaction problems [64]. Similar to these works, our proposed approaches are also based on GNNs. Our centralized solver follows the methodology in [44] with additional modifications to account for the weights associated with the vertices, and improves search efficiency through 1-step look-ahead rollout search guided by a fast heuristic. Moreover, the aforementioned works [43], [44], [61]–[63] propose centralized solutions whereas, to the best of our knowledge, we provide the first fully distributed GCN-based solution to the MWIS problem.

III. SYSTEM MODEL AND PROBLEM STATEMENT

A. System Model

Consider a wireless multi-hop network as illustrated in Fig. 1(a), where the existence of link (i, j) implies that user i and user j can communicate with each other. Since we will ultimately focus on a conflict graph whose vertices represent links in the wireless network, we denote an arbitrary link (i, j) as v . A flow f describes the stream of packets from a source user to a destination user. A flow may pass through multiple links determined by a routing scheme. For each link, there is a queuing system q for packets of all the flows.

The wireless network adopts a multiple access scheme that divides the spectrum resource into a set of orthogonal sub-channels, $\mathcal{K} = \{1, \dots, K\}$, and time slots. The wireless channel is assumed to be stationary and ergodic network wide, and invariant within a time slot, i.e., the coherence time of the channel is assumed to exceed the duration of a time slot. In Fig. 1(b), an example of a frequency division multiple access (FDMA) system is illustrated.¹ The channel state information of link v on sub-channel k at time slot t is denoted by $h_t^k(v)$. We assume an orthogonal access scheme where each slot of the spectral-temporal grid in Fig. 1(b) can only be accessed by one link out of a set of potentially interfering links.

There are two formulations of interference constraints in the literature: physical distance model and hop distance model [23]. In this work, the interference in the system is considered to follow a physical distance model. For example, two links interfere with each other if their incident users are within a certain distance such that their simultaneous transmission will cause the outage probability to exceed a certain level. Depending on the air-interface technology and antenna systems, the interference zone of a link can be different from its connectivity zone. A link is assumed to be able to learn its interfering neighbors by monitoring the channel and/or beacon signals. Moreover, mutually interfering links are assumed to be able to exchange control messages, e.g., with low-rate modulation and coding schemes. Notice that, in principle, the interference zone of a link would depend on the transmit power of the corresponding user and hence possibly vary with time. To simplify the analysis and avoid this dependence, we consider the scenario in which all the users transmit at power levels that do not vary with time. In general, our approaches work on any conflict graph, no matter how it is constructed.

B. Single-Radio Single-Channel Scheduling

We first consider a wireless network with only one sub-channel, in which each user is equipped with one half-duplex radio interface. The interference relationship between links of the wireless multi-hop network is described by a *conflict graph* \mathcal{G} , where a vertex in the conflict graph represents a link in the wireless network and the presence of an edge in \mathcal{G} encodes the fact that the corresponding links interfere with each other. In the rest of this paper, we focus on the conflict graph \mathcal{G} which we assume to be known; see, e.g., [65] for its estimation. Recall that an independent (vertex) set in a graph

¹Alternatively, in code division multiple access (CDMA) systems, channels are implemented by orthogonal codes.

is a set of vertices such that no two vertices in the set are neighbors of each other. From the definition of \mathcal{G} , only wireless links that form independent sets (IS) in \mathcal{G} can communicate simultaneously in time and frequency under the constraint of orthogonal access.

The state of the system at time slot t can be described by the tuple $(\mathcal{G}_t, \mathbf{q}_t, \mathbf{f}_t, \mathbf{h}_t)$ consisting of the conflict graph \mathcal{G}_t , queue lengths \mathbf{q}_t , flows \mathbf{f}_t , and channel states \mathbf{h}_t . Since the scheduling is conducted at each time slot t , for notational simplicity we omit the subscript t , denoting the system state as $(\mathcal{G}, \mathbf{q}, \mathbf{f}, \mathbf{h})$. In this setting, the task of optimal link scheduling can be described as selecting a set of non-interfering links, $\mathbf{v} \subseteq \mathcal{V}$, to transmit in order to maximize some utility $u(\mathbf{v}) = f(\mathbf{v}; \mathcal{G}, \mathbf{q}, \mathbf{f}, \mathbf{h})$ that is parameterized by the current state of the system. As is customary [4], we model here the utility of the set of links \mathbf{v} (or the set of vertices in the conflict graph) as the sum of utilities associated with each link, i.e., $u(\mathbf{v}) = \sum_{v \in \mathbf{v}} u(v)$, leading to the following formal problem statement.

Problem 1. Consider a conflict graph $\mathcal{G}(\mathcal{V}, \mathcal{E})$, where \mathcal{V} and \mathcal{E} describe all the links and their conflict relationships in the wireless network, respectively, and a utility function $u : \mathcal{V} \rightarrow \mathbb{R}_+$. The optimal scheduling is given by selecting a subset of vertices $\mathbf{v}^* \subseteq \mathcal{V}$ such that

$$\mathbf{v}^* = \operatorname{argmax}_{\mathbf{v} \subseteq \mathcal{V}} \sum_{v \in \mathbf{v}} u(v) \quad (1a)$$

$$\text{s.t. } (v_i, v_j) \notin \mathcal{E}, \forall v_i, v_j \in \mathbf{v}. \quad (1b)$$

From the statement of Problem 1, it becomes evident that we have transformed the optimal scheduling at each temporal slot to an MWIS problem in the corresponding conflict graph. Indeed, we want to choose non-neighboring vertices in the conflict graph (i.e., non-interfering links in the wireless network) such that the total utility is maximized. As discussed in Section I and formally introduced here, this utility u is a function of the current state of the network with many existing variants [3], [4], [6], [10], [17], [18]. The *MaxWeight* scheduler described by Problem 1 is agnostic to the specific choice of this utility function.

C. Multi-Channel Scheduling

There are at least two ways to extend the *MaxWeight* scheduler defined in Problem 1 to networks with a set of orthogonal sub-channels \mathcal{K} : 1) Sequentially solve a set of single-channel scheduling tasks with state $(\mathcal{G}^k, \mathbf{q}, \mathbf{f}, \mathbf{h}^k)$ for each sub-channel $k \in \mathcal{K}$, where the queue lengths \mathbf{q} for sub-channel k depend on the schedules on sub-channels $\{1, \dots, k-1\}$. The complexity and scheduling overhead of this approach grows linearly with the number of channels K . 2) Solve the MWIS problem on a single multi-channel conflict graph, for which detailed construction methods can be found in [66], [67]. The multi-channel conflict graph is K times larger than the single-channel conflict graph. With a heuristic solver of logarithmic complexity, the second approach can reduce the complexity from $\mathcal{O}(K \log V)$ to $\mathcal{O}(\log KV)$ at the cost of poorer relative performance on larger graphs as illustrated in Section VI-B. In this paper, we focus on single-channel scheduling while

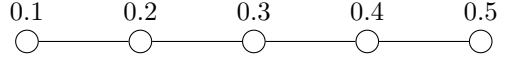


Fig. 2: An example path graph with 5 vertices of increasing weights on which LGS requires 5 iterations to complete as the worst case.

numerically evaluating the second approach for multi-channel scheduling.

D. Greedy Heuristics

A centralized greedy solver (CGS) builds the estimate $\hat{\mathbf{v}}_{\text{Gr}}$ approximating the solution to (1) in an iterative fashion by first adding to $\hat{\mathbf{v}}_{\text{Gr}}$ the vertex with the largest utility, deleting its neighbors as potential candidates, and repeating this procedure until all vertices are either added to $\hat{\mathbf{v}}_{\text{Gr}}$ or deleted. Specifically, the partial solution and residual graph are initialized as $\hat{\mathbf{v}}_{\text{Gr}} = \emptyset$ and $\mathcal{G}'(\mathcal{V}', \mathcal{E}') = \mathcal{G}(\mathcal{V}, \mathcal{E})$, respectively. In each iteration, the CGS grows the partial solution as

$$\hat{\mathbf{v}}_{\text{Gr}} \leftarrow \hat{\mathbf{v}}_{\text{Gr}} \cup \{v\}, \text{ where } v = \operatorname{argmax}_{v_i \in \mathcal{V}'} u(v_i), \quad (2)$$

and then update the residual graph as $\mathcal{G}' \leftarrow \mathcal{G}' \setminus (\hat{\mathbf{v}}_{\text{Gr}} \cup \mathcal{N}(\hat{\mathbf{v}}_{\text{Gr}}))$, where $\mathcal{N}(v)$ contain all vertices that are neighbors to some vertex in the set v . The algorithm terminates when \mathcal{G}' is empty ($\mathcal{G}' = \emptyset$), and then outputs $\hat{\mathbf{v}}_{\text{Gr}}$ as the full solution.

The distributed implementation of (2) is denominated as local greedy solver (LGS) [17], in which vertex v is added to the solution set if its weight is the largest in the neighborhood,

$$v \in \hat{\mathbf{v}}_{\text{Gr}}, \text{ if } u(v) > \max_{v_i \in \mathcal{N}(v)} u(v_i). \quad (3)$$

In practice, the LGS has a built-in tie-breaking mechanism based on an initial assignment of identification numbers to each vertex in the conflict graph that does not require additional information exchanges in the case of a tie. A vertex added to $\hat{\mathbf{v}}_{\text{Gr}}$ marks itself as $+1$ and broadcasts a control message to its neighbors, who then mark themselves as -1 . Then, the unmarked vertices form the residual graph \mathcal{G}' . Notice that these local exchanges are between vertices in the conflict graph. By construction, $\hat{\mathbf{v}}_{\text{Gr}}$ from CGS or LGS is guaranteed to follow the IS constraint in (1b) but the suboptimality gap $u(\mathbf{v}^*) - u(\hat{\mathbf{v}}_{\text{Gr}})$ might be large since these greedy heuristics do not fully consider the topology of \mathcal{G} .

Both CGS and LGS have a linear computational complexity $\mathcal{O}(V)$. However, as distributed MWIS solvers are parallel by nature, we focus on their local complexity. The LGS has a logarithmic average local complexity $\mathcal{O}(\log V)$ on random graphs and a linear worst-case complexity $\mathcal{O}(V)$ on path graphs with increasing vertex weights along the path as illustrated in Fig. 2 [17].

IV. GRAPH CONVOLUTIONAL NETWORK-GUIDED TREE SEARCH

Our centralized MWIS solvers are based on a GCN-guided tree search, which estimates an approximate solution $\hat{\mathbf{v}}_{\text{GCN}}$ by iteratively adding one vertex at a time under the guidance of a GCN without violating the constraint of independent set in (1b). Our methodology consists of defining a search tree of candidate solutions and then traversing it with multiple strategies under a unified iterative framework, detailed as follows.

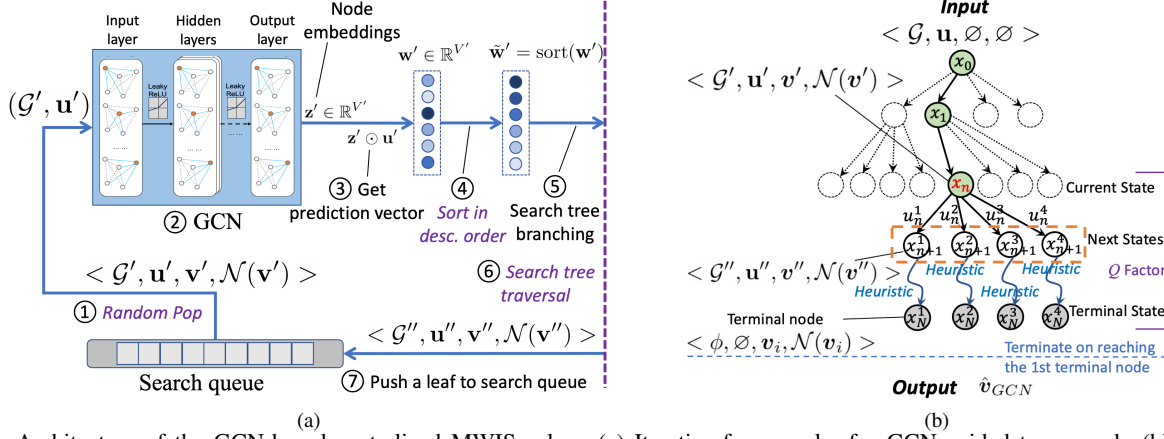


Fig. 3: Architecture of the GCN-based centralized MWIS solver. (a) Iterative framework of a GCN-guided tree search. (b) 1-step rollout search that can quickly reach a good terminal node on the search tree.

A. Iterative Framework

The iterative algorithmic framework, as illustrated in Fig. 3, is inspired by the methodology for the unweighted MIS problem from [44]. The possible state transitions of each iteration form a search tree, as illustrated in Fig 3(b), which we explain in more detail in this section. The solver finds an approximate solution by traversing from the root of the search tree to a terminal node. A node in the search tree is described by the tuple $\langle \mathcal{G}', \mathbf{u}', \mathbf{v}', \mathcal{N}(\mathbf{v}') \rangle$ representing an intermediate search state, where \mathcal{G}' is the residual graph, \mathbf{u}' is the corresponding residual utility vector collecting the utilities $u(v)$ for all $v \in \mathcal{G}'$, \mathbf{v}' is the partial solution for \mathcal{G} , and $\mathcal{N}(\mathbf{v}')$ is the set of all the vertices adjacent to some vertex in the partial solution. The root node of the search tree $\langle \mathcal{G}, \mathbf{u}, \emptyset, \emptyset \rangle$, as the initial state, is generated from the input conflict graph \mathcal{G} and corresponding utility vector \mathbf{u} . At a terminal node, the residual graph is empty $\mathcal{G}' = \phi$ and \mathbf{v}' is a feasible approximate solution to Problem 1.

On initialization, the root node is pushed into the search queue. In each iteration, the solver expands a (non-terminal) node randomly popped from the queue, and proceeds to one of its children in 7 steps, as illustrated in Fig. 3(a). In step 1, a non-terminal node $\langle \mathcal{G}', \mathbf{u}', \mathbf{v}', \mathcal{N}(\mathbf{v}') \rangle$ is randomly popped from the search queue, whose enclosed residual graph \mathcal{G}' and residual utility vector \mathbf{u}' are fed into the GCN. In step 2, based on the inputs of \mathcal{G}' and \mathbf{u}' , the GCN generates the node embedding vector $\mathbf{z}' \in \mathbb{R}^{V'}$, which contains the topology-aware scaling factor $\mathbf{z}'_v = \mathbf{z}'(v)$ for all $v \in \mathcal{V}'$, as $\mathbf{z}' = \Psi_{\mathcal{G}'}(\mathbf{u}'; \Xi)$, and $\Psi_{\mathcal{G}'}$ is an L -layered GCN defined on the graph \mathcal{G}' (as detailed in Section IV-B), \mathbf{u}' is the residual utility vector, and Ξ represents the collection of trainable parameters of the GCN. In step 3, a prediction vector is created through the element-wise product $\mathbf{w}' = \mathbf{z}' \odot \mathbf{u}'$, where an element $\mathbf{w}'_v = w'(v)$ represents the topology-aware utility of vertex v . In step 4, the prediction vector \mathbf{w}' is sorted in descending order as illustrated in Fig. 3(a), where the elements in \mathbf{w}' and its sorted version $\tilde{\mathbf{w}'}$ with larger values are represented by darker colors. Next, in step 5, B prediction vertices are extracted from $\tilde{\mathbf{w}'}$ to create the B branches (next states) of the current node (current state) in the search tree; see. Fig. 3(b). The branching factor B is further discussed in Sections IV-C and IV-D. The child node $\langle \mathcal{G}'', \mathbf{u}'', \mathbf{v}'', \mathcal{N}(\mathbf{v}'') \rangle$ on a branch is generated

based on one of the B prediction vertices, denoted as v , as:

$$\mathcal{G}'' = \mathcal{G}' \setminus (v \cup \mathcal{N}(v)), \mathbf{v}'' = \mathbf{v}' \cup \{v\}. \quad (4)$$

In step 6, the solver selects one of the B children nodes to continue processing according to a certain traversal strategy, as detailed in Sections IV-C and IV-D. Lastly, in step 7, if the selected child node (next state) is a non-terminal node, it is pushed into the search queue.

B. Graph Convolutional Network Design

Our GCN has an L -layer structure as follows: Given the input feature as $\mathbf{X}^0 = \mathbf{u}'$, then $\mathbf{z}' = \Psi_{\mathcal{G}'}(\mathbf{u}'; \Xi) = \mathbf{X}^L$, where an intermediate l th layer of the GCN is given by

$$\mathbf{X}^l = \sigma_l(\mathbf{X}^{l-1} \Theta_0^l + \mathcal{L} \mathbf{X}^{l-1} \Theta_1^l). \quad (5)$$

In (5), \mathcal{L} is the normalized Laplacian of \mathcal{G} , $\Theta_0^l, \Theta_1^l \in \mathbb{R}^{g_{l-1} \times g_l}$ are the trainable parameters, g_{l-1} and g_l are the dimensions of the output features of layers $l-1$ and l , respectively, and $\sigma_l(\cdot)$ is the activation function. The dimension of the input feature is $g_0 = 1$. The activation functions of the input and hidden layers are selected as leaky ReLUs. By setting the dimension of the output layer as $g_L = 1$ with linear activation, the GCN generates a node embedding vector, $\mathbf{z}' \in \mathbb{R}^{V'}$, as a topological scaling factor. As explained, the prediction vector is then computed as $\mathbf{w}' = \mathbf{z}' \odot \mathbf{u}'$. The GCN is trained by RL with the help of an efficient CGS. Since this training mechanism is shared with our proposed distributed solution, we defer its explanation to Section V-B.

C. GCN-guided Centralized Rollout Search

In order to reach a good solution, the branching factor B should be configured to create a large search tree with a large search space. In the approach outlined so far, it may take a long time for the solver to find a good terminal node in a large search space. To reach a good terminal node quickly, we introduce GCN-guided centralized rollout search (GCN-CRS), which employs 1-step rollout search [68] to further guide the tree search, as illustrated in Fig. 3(b). The B branches are given by the indices of the first B vertices in $\tilde{\mathbf{w}'}$. We define a Q function whose value estimates the quality of a node in the search tree. At iteration n , the GCN-CRS estimates the Q

values of the B children nodes of the current state x_n through 1-step rollout, i.e., the Q value of the b th child node x_{n+1}^b is

$$Q(x_{n+1}^b) = u_n^b + f_h(x_{n+1}^b), b \in \{1, \dots, B\}. \quad (6)$$

The immediate reward $u_n^b = u(v_b)$ of transitioning from the current state x_n to the next state x_{n+1}^b is the utility of the predicted vertex v_b that generates the child node x_{n+1}^b . The score of the b th child node $f_h(x_{n+1}^b)$ is the total utility obtained by an efficient *guiding heuristic* traversing from state x_{n+1}^b to a terminal state. The GCN-CRS proceeds to the child node with the largest Q value, and ties are broken randomly. In GCN-CRS, the search queue in Fig. 3(a) is essentially bypassed, and the search tree is traversed along a single path and terminated when it reaches the first terminal node. The training method of the GCN is detailed in Section V-B.

The performance of the GCN-CRS is guaranteed to be no worse than (and largely dictated by) the guiding heuristic [68]. In our case, the CGS is selected as the guiding heuristic due to its linear complexity and determinism. Specifically, the score of the b th child node is obtained as $f_h(x_{n+1}^b) = u(v_{Gr}^b)$, where v_{Gr}^b is obtained by either the vanilla CGS based on graph $\mathcal{G}_b'' = \mathcal{G}' \setminus (v_b \cup \mathcal{N}(v_b))$ and weights \mathbf{u}_b'' , or an enhanced CGS based on \mathcal{G}_b'' and weights $\mathbf{w}' \setminus \{w(v_i), v_i \in (v_b \cup \mathcal{N}(v_b))\}$, where \mathcal{G}' and \mathbf{w}' are obtained from the state x_n . Moreover, the rollouts on the B branches can be parallelized. The GCN-CRS solvers using vanilla CGS and enhanced CGS as guiding heuristics are denoted as GCN-CRS-v and GCN-CRS-e, respectively.

D. Reference GCN-guided Centralized Solvers

Next, we propose two reference solvers with which to compare GCN-CRS: GCN-guided centralized random tree search (GCN-CRTS) and GCN-guided centralized greedy search (GCN-CGS). These are obtained by modifying the state-of-the-art solvers for the unweighted MIS problem in [44] and [43], respectively, making them compatible with our MWIS setting.

The idea of GCN-CRTS is to reach as many random terminal nodes as possible in a given time interval to increase its chance of finding a good solution from them. The GCN-CRTS is almost identical to the MIS solver in [44], in which a node embedding matrix $\mathbf{Z}' \in [0, 1]^{V' \times B}$ is generated by a GCN with a slightly different output structure, with only two modifications: 1) Using $\mathbf{W}' = \mathbf{Z}' \odot \mathbf{u}' \mathbf{1}^\top$ instead of \mathbf{Z}' as the prediction matrix. 2) For computational efficiency, synthetic random graphs are used as the training data for supervised learning, where the label vectors are generated by heuristics instead of exactly solving the NP-hard problem. Specifically, the labels are generated by selecting the best solution from two guiding heuristics: linear programming [69] and centralized greedy solver. The implementation of the GCN-CRTS is detailed in Section I of the Supplemental Material [70].

The GCN-CGS is modified from the deep Q network in [43] by replacing the Node2Vec module with a GCN. For a non-terminal node $\langle \mathcal{G}', \mathbf{u}', \mathbf{v}', \mathcal{N}(\mathbf{v}') \rangle$ in the search tree, the GCN takes $(\mathcal{G}', \mathbf{u}')$ as input and generates node embedding $\mathbf{z}' \in \mathbb{R}^{V'}$ as the Q values of the action space $\mathcal{A}' = \mathcal{V}'$, whereas the branching factor $B = |\mathcal{V}'|$ is no longer a hyperparameter. The action is selected by an ϵ -greedy method. The next state

TABLE I: Computational complexity of centralized MWIS solvers

Algorithm	Complexity
CGS	$\mathcal{O}(V)$
GCN-CRTS	$\mathcal{O}(LV^2g^2B^V)$
GCN-CGS	$\mathcal{O}(LV^2g^2)$
GCN-CRS	$\mathcal{O}(LV^2g^2 + BV^2/\bar{d})$

$(\mathcal{G}'', \mathbf{u}'')$ is generated according to (4). The search terminates upon reaching a terminal node. The GCN is trained by finite-horizon deep Q learning with experience replay, where the discount rate is set as 1.0. The reward is defined as $\gamma = 0$ for a non-terminal state, and $\gamma = u(\hat{v}_{GCN})/u(\hat{v}_{Gr})$ for a terminal state, where \hat{v}_{Gr} and \hat{v}_{GCN} are the full solutions for input $(\mathcal{G}, \mathbf{u})$ obtained by vanilla CGS and GCN-CGS, respectively. The exploration rate ϵ is initialized to 1 and decays exponentially during training, and set to 0 for testing and deployment. More details of the implementation can be found in Section II of the Supplemental Material [70].

Both GCN-CRTS and GCN-CGS benefit from the flexible input dimensions of GCN and the iterative algorithmic framework, so that they can generalize to large graphs and outperform the training heuristics [44]. The GCN-CGS can reach a good terminal node quickly. However, the GCN-CRTS will take a relatively long time to find a good solution (e.g., several minutes), and therefore not suitable for link scheduling.

E. Computational Complexity

The computational complexity of the l th layer of the GCN is $\mathcal{O}(\bar{d}Vg_lg_{l-1})$, where \bar{d} is the average degree of a vertex in the input graph. By assuming $g_l = g, \forall l \in \{1, \dots, L\}$, an L -layered GCN has a computational complexity of $\mathcal{O}(LVg^2\bar{d})$. In tree search, reaching a terminal node requires an average of V/\bar{d} steps, therefore the computational complexity of finding a solution is $\mathcal{O}(LV^2g^2)$. Without timeout, the GCN-CRTS requires an exponential complexity of $\mathcal{O}(LV^2g^2B^V)$ to reach all B^V terminal nodes. To find a good solution on graphs of hundreds of vertices, a timeout of several minutes is usually required for GCN-CRTS. The computational complexity of GCN-CRS is $\mathcal{O}(LV^2g^2 + BV^2/\bar{d})$, since the guiding heuristic of CGS will be executed B times on each node of the search tree, adding a complexity of $\mathcal{O}(BV^2/\bar{d})$ with an average of V/\bar{d} passes. The computational complexities of the presented centralized MWIS solvers are summarized in Table I.

V. DISTRIBUTED MWIS SOLVER USING GRAPH NEURAL NETWORKS

Our goal in the design of a distributed solver is to *decrease the suboptimality gap of the baseline LGS described in Section III-D while keeping its two main advantages*: 1) Low computational complexity, and 2) Can be implemented in a distributed manner with low communication cost. To achieve this goal, LGS with modified weights is proposed to solve Problem 1. More precisely, mimicking the development of our centralized solvers, instead of considering the vanilla utilities $u(v)$ we consider graph-aware utilities $w(v) = z(v)u(v)$, where the scalar node embedding $z(v)$ encodes a relevant topological feature of vertex v . Intuitively, if vertex v is a central link that may interfere with many other links in the

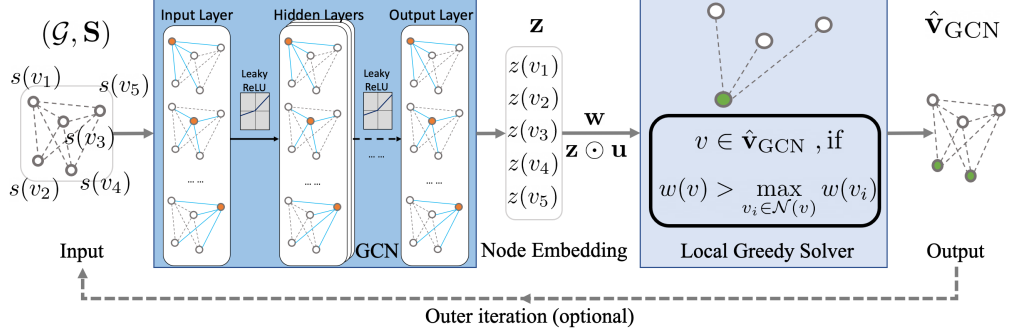


Fig. 4: Architecture of the GCN-based distributed MWIS solver. First, the conflict graph \mathcal{G} and node features \mathbf{S} are encoded into the scalar embeddings \mathbf{z} via a GCN. Then, the element-wise product of \mathbf{z} and \mathbf{u} is fed into a local greedy algorithm to generate a solution $\hat{\mathbf{v}}_{\text{GCN}}$.

wireless network, then $z(v)$ should downscale the utility $u(v)$ since scheduling v would preclude many other links from the schedule. By contrast, if vertex v is peripheral in the conflict graph \mathcal{G} (e.g., an isolated link in the original wireless network) then $z(v)$ should amplify $u(v)$. In summary, $z(v)$ should be a topology-aware scaling that reduces the MWIS suboptimality gap and, to be consistent with our goal, should also be attainable in a distributed manner with low communication and computational cost. With these requirements in mind, we propose to obtain a vectorized node embedding $\mathbf{z} \in \mathbb{R}^V$ collecting $z(v)$ for all $v \in \mathcal{V}$ as the output of a GCN [39]. The distributed MWIS solver composed of a distributed GCN followed by LGS is denoted by *GCN-LGS*. The architecture of the GCN-LGS solver is illustrated in Fig. 4. As detailed later, the training of GCN-LGS is centralized while its deployment is distributed.

A. Distributed Architecture

In accordance with Problem 1, the inputs to the GCN-LGS solver consist of the conflict graph \mathcal{G} and a feature matrix \mathbf{S} , and the output of the solver is an estimate $\hat{\mathbf{v}}_{\text{GCN}}$ of the optimal link scheduling. The feature matrix \mathbf{S} can be the utility vector \mathbf{u} , a constant vector $\mathbf{1}$ (featureless case), or contain other vertex features.

The first step is to obtain a topology-aware node embedding $\mathbf{z} \in \mathbb{R}^V$, as $\mathbf{z} = \Psi_{\mathcal{G}}(\mathbf{S}; \Xi)$, where $\Psi_{\mathcal{G}}$ is an L -layered GCN defined on \mathcal{G} as described in (5). The GCN is configured with a linearly activated output layer, and $g_L = 1$. Since the normalized Laplacian \mathcal{L} is a local operator on \mathcal{G} , it should be noted that $z(v)$ can be computed locally at each vertex v through L rounds of local exchanges with its neighbors. As an extreme case, a 1-layer GCN with input $\mathbf{S} = \mathbf{u}$ does not employ any non-linear activation and the node embedding $z(v)$ can be locally computed as

$$z(v) = u(v) \theta_0 + \left(u(v) - \sum_{v_i \in \mathcal{N}(v)} \frac{u(v_i)}{\sqrt{d(v)d(v_i)}} \right) \theta_1, \quad (7)$$

where $\mathcal{N}(v)$ denotes the neighbor set of vertex v , and $d(\cdot)$ is the degree of a vertex. In practice, a link v can track its degree by counting its interfering neighbors during local exchanges. The expression in (7) shows that the local computational complexity of link v scales linearly with its degree, which is small in many practical scenarios. The major complexity of GCN-LGS comes from local exchanges.

Next, the element-wise product between \mathbf{z} and \mathbf{u} is computed to obtain a set of modified graph-aware utilities $\mathbf{w} = \mathbf{z} \odot \mathbf{u}$. The estimated solution $\hat{\mathbf{v}}_{\text{GCN}}$ is obtained from \mathbf{w} through the LGS [17] detailed in Section III-D.

B. Centralized Training

Having discussed the rationale and the mechanics of the proposed architecture, we are left to discuss how to train the parameters Ξ in the GCN. It should be noted that there are two main differences between the proposed distributed setting and the typical supervised or semi-supervised settings on which GCNs are employed. First, although the training inputs $(\mathcal{G}, \mathbf{u})$ can be simulated, in general their associated optimal outputs \mathbf{v}^* cannot be obtained since this would require solving an NP-hard problem. Second, the output \mathbf{z} of the GCN is related to the objective to be maximized $u(\hat{\mathbf{v}}_{\text{GCN}})$ through a non-differentiable local greedy process. Inspired by RL techniques, we seek to overcome these limitations by introducing a reward γ for $v \in \hat{\mathbf{v}}_{\text{GCN}}$, where $\hat{\mathbf{v}}_{\text{GCN}}$ can be viewed as the set of actions selected by LGS based on $(\mathcal{G}, \mathbf{w})$. Hence, we define the target vector ρ as

$$\rho(v) = \begin{cases} \gamma, & v \in \hat{\mathbf{v}}_{\text{GCN}} \\ z(v), & v \notin \hat{\mathbf{v}}_{\text{GCN}} \end{cases}, \quad \text{where } \gamma = \frac{u(\hat{\mathbf{v}}_{\text{GCN}})}{u(\hat{\mathbf{v}}_{\text{Gr}})}. \quad (8)$$

Notice that $\hat{\mathbf{v}}_{\text{GCN}}$ and $\hat{\mathbf{v}}_{\text{Gr}}$ are the full solutions for input $(\mathcal{G}, \mathbf{u})$ obtained respectively by GCN-LGS being trained and the efficient baseline CGS, thus circumventing the need to exactly solve the MWIS problem. Intuitively, whenever the inclusion of v in $\hat{\mathbf{v}}_{\text{GCN}}$ leads to a solution with higher utility than the greedy baseline [i.e., $u(\hat{\mathbf{v}}_{\text{GCN}}) > u(\hat{\mathbf{v}}_{\text{Gr}})$], vertex v should be rewarded. By contrast, whenever vertex v is included in a bad solution [$u(\hat{\mathbf{v}}_{\text{GCN}}) < u(\hat{\mathbf{v}}_{\text{Gr}})$], it is punished to avoid its inclusion in future solution sets. Accordingly, the following root-mean-square loss is proposed to train our GCN

$$\ell(\Xi; \mathcal{G}, \mathbf{u}) = \sqrt{\frac{1}{V} \sum_{v \in \mathcal{V}} (z(v) - \rho(v))^2}. \quad (9)$$

By drawing graphs and utility vectors from prescribed distributions, we collect the tuple $<(\mathcal{G}_i, \mathbf{u}_i), \mathbf{z}_i, \hat{\mathbf{v}}_{\text{GCN},i}, \gamma_i>$ of each forward pass i to the experience buffer, and then train the parameters Ξ of the GCN through experience replay, employing the Adam optimizer and exponentially decaying learning rates.

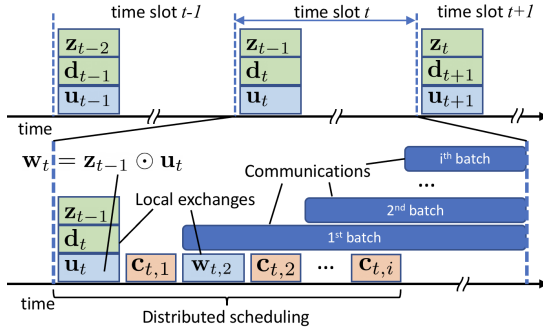


Fig. 5: Timeline of distributed scheduling with messages of 1-layer GCN piggybacked on the local exchanges of original LGS. By reusing z_{t-1}^G , the GCN-LGS has the same local complexity of LGS.

C. Architectural Variations

Apart from the aforementioned baseline architecture, the GCN-LGS admits several useful variations. The first set of variations is associated with the iterative structure, as illustrated in Fig. 4. First, the baseline LGS can be truncated to N iterations, denoted as *GCN-LGS- N* , in order to achieve a constant local complexity at the cost of the quality of solution, which is a key aspect to promote scalability since the constant local complexity is independent of the graph size V . On the other hand, the GCN can be placed before each inner iteration of LGS (i.e., the step in (3)), which is denoted as *GCN-LGS-it*, so that the input of the LGS iteration $w' = z' \odot u'$, where $z' = \Psi_{G'}(u'; \Xi)$, is based on the residual graph (G', S') from the previous iteration, rather than the input graph (G, S) as in the baseline GCN-LGS. The GCN-LGS-it can further improve the performance over the baseline GCN-LGS at the cost of higher local complexity.

The second variation refers to the choice of input features as $S = \mathbf{1}$. We can think of the node embedding $z = \Psi_G(\mathbf{1}; \Xi)$ generated by a featureless GCN as a *topological embedding*, denoted as z^G , which can be reused until the network topology changes. In practice, z^G can be reused for a coherent window of T time slots that matches the pace of topological change to further reduce the computational and communication complexities of distributed scheduler.

Moreover, by reusing the topological embedding generated L time slots before, i.e., use $w_t = z_{t-L}^G \odot u_t$ in time slot t , the additional local complexity of GCN for GCN-LGS can be reduced to zero, since z_{t-L}^G and the intermediate features X^l can be piggybacked to the local exchange of d_t and u_t at the beginning of time slot t . An exemplary GCN-LGS with 1-layer GCN and $w_t = z_{t-1}^G \odot u_t$ is illustrated in Fig. 5. Compared to LGS, this GCN-LGS only incurs larger control messages for the first round of local exchange, additional local computational complexity, and slightly topological mismatch between consecutive time slots. The robustness of GCN-LGS to topological mismatch is evaluated in Section VI-A.

Note that a scheduled link in LGS can start to transmit right after broadcasting a control message $c_{t,i}$ to mute its interfering neighbors, without the need to wait until every link in the network is determined or until a maximum number of local exchanges is reached. Under this scheme, the impact of the scheduling overhead of LGS (and GCN-LGS) to spectrum utilization efficiency is further reduced without truncation.

TABLE II: Local complexity of distributed MWIS solvers

Algorithm	Worst	Average
Local greedy solver (LGS) [17]	$\mathcal{O}(V)$	$\mathcal{O}(\log V)$
Threshold local greedy [18]	$\mathcal{O}(\log_\alpha(\beta V))$	$\mathcal{O}(\log_\alpha(\beta V))$
Message passing [6]	$\mathcal{O}(V)$	$\mathcal{O}(V)$
Ising [21]	const. $\sim 10^2$	const. $\sim 10^2$
GCN-LGS	$\mathcal{O}(L + V)$	$\mathcal{O}(L + \log V)$
GCN(reuse)-LGS	$\mathcal{O}(V)$	$\mathcal{O}(\log V)$
GCN-LGS- N	$\mathcal{O}(L + N)$	$\mathcal{O}(L + N)$
GCN-LGS-it	$\mathcal{O}((L + 1)V)$	$\mathcal{O}((L + 1)\log V)$

D. Local Communication Complexity

Without reusing the topological embedding, the average local complexity of the GCN-LGS solver is $\mathcal{O}(L + \log V)$, where $\mathcal{O}(L)$ is the local complexity of the GCN and $\mathcal{O}(\log V)$ is the average local complexity of LGS (as discussed in Section III-D). For LGS truncated to N iterations, the local complexity of GCN-LGS- N is $\mathcal{O}(L + N)$. In this way, \hat{v}_{GCN} can be computed in a distributed manner, where the local computational and communication costs can be controlled by modifying the number of layers L in the GCN. Moreover, with reusable topological embedding, the average local complexity of GCN-LGS is $\mathcal{O}(\log V)$ with zero additional complexity. The worst and average local complexities of the baseline and proposed distributed MWIS solvers are listed in Table II.

VI. NUMERICAL EXPERIMENTS

The performance of the GCN-based MWIS solvers is evaluated in synthetic random graphs and as schedulers in wireless networks. The comparative baselines are CGS, LGS [17] and message passing (MP) [6]. The quality of an approximate solution \hat{v} is evaluated by its approximation ratio (AR) $u(\hat{v})/u(v^*)$, where the optimal solution v^* is obtained by solving the computationally expensive integer programming formulation of MWIS [6], [19] using the Gurobi solver [54].

The synthetic graphs for training and testing are generated from the Erdős–Rényi (ER) [71] and Barabási–Albert (BA) [72] models. The ER model is completely determined by two parameters: the number of vertices V , and the probability of edge-appearance p . The BA model is also determined by two parameters: the number of vertices V and the number of edges, m , that each new vertex forms during the preferential attachment process. In the experiments, we set $m = Vp = \bar{d}$ so that graphs from the ER and BA models have the same expected average degree. By default, the vertex utilities are drawn following a uniform distribution $u(v) \sim \mathbb{U}(0, 1)$.

The hyperparameters of the evaluated GCNs are as follows: the numbers of layers $L \in \{1, 5, 20\}$, the size of every hidden layer is $g_l = 32$ for $L > 1$. The L -layered GCN is denoted as $\text{GCN}(L)$. The branching factor is $B = 32$. Each GCN is trained on a set of 5900 random graphs drawn from an ER model unless otherwise specified. The training set comprises 5000 graphs of size $V \in \{100, 150, 200, 250, 300\}$ and expected average degree $\bar{d} \in \{2, 5, 7.5, 10, 12.5\}$ (200 graphs per (V, \bar{d})), and 900 graphs of size $V \in \{30, 100\}$ and edge probability $p \in \{0.1, 0.2, \dots, 0.9\}$ (50 graphs per (V, p)). The timeout of GCN-CRTS is set to 5 minutes. The GCN in GCN-CRTS is trained by supervised learning with a maximum

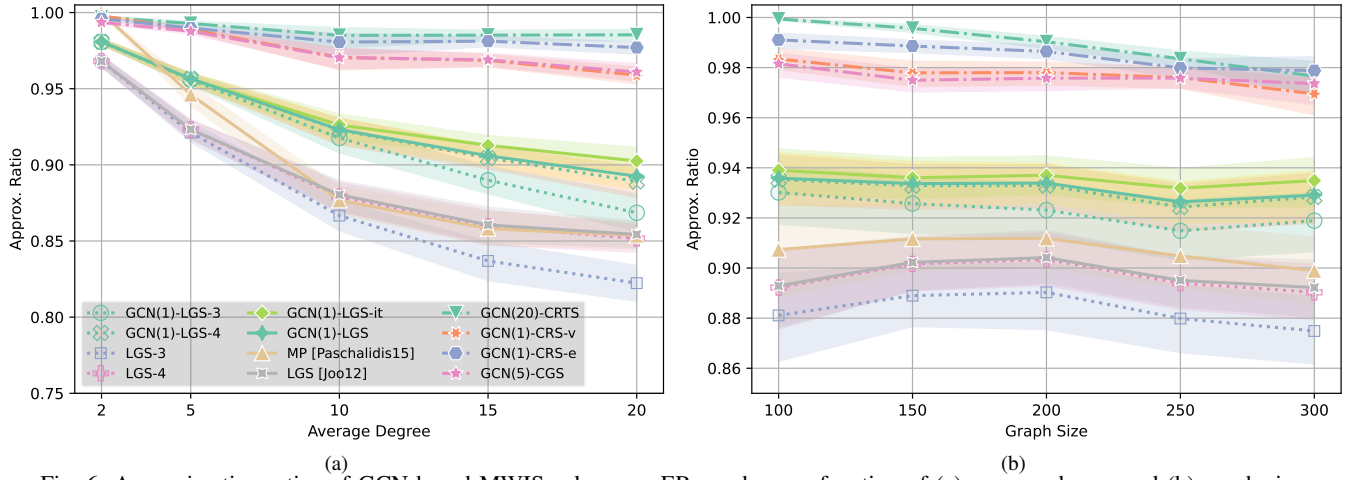


Fig. 6: Approximation ratios of GCN-based MWIS solvers on ER graphs as a function of (a) average degree and (b) graph size.

TABLE III: Mean ARs of solvers on synthetic graphs

Solver	Training set	ER set	BA set	Thpt.
CGS, LGS [Joo12]	-	0.897	0.858	0.921
MP [Paschalidis15]	-	0.907	0.892	-
GCN(20)-CRTS	ER	0.989	0.993	-
GCN(5)-CGS	ER	0.976	0.972	0.960
GCN(1)-CRS-v	ER	0.977	0.973	0.995
GCN(1)-CRS-e	ER	0.985	0.986	0.996
GCN(1)-LGS	ER	0.932	0.937	0.954
GCN(1)-LGS-it	ER	0.936	0.942	0.956

of 200 epochs as explained in Section I-D of the Supplemental Material [70]. The GCNs in GCN-CRS and GCN-LGS are trained as described in Section V-B, for which the settings include a batch size of 200 for experience replay, 25 epochs, and periodic gradient reset. The same training configuration is used for the training of GCN-CGS as described in Section II of the Supplemental Material [70].²

A. Performance on Synthetic Random Graphs

1) *Results on ER graphs:* First, the GCN-based MWIS solvers, baseline heuristics, and optimal solver are tested on a set of 500 ER graphs of size $V \in \{100, 150, 200, 250, 300\}$ and average degree $\bar{d} \in \{2, 5, 10, 15, 20\}$, with 20 instances for each pair of (V, \bar{d}) . The average ARs of the tested solvers are listed in Table III (under the ‘ER set’ column) for the entire test set, and illustrated in Figs. 6(a) and 6(b) as a function of the average degree and size of the tested graphs, respectively. Note that the same trained GCN model of GCN(1) is used by solvers of GCN(1)-CRS-v, GCN(1)-CRS-e, GCN(1)-LGS, GCN(1)-LGS-it, and GCN(1)-LGS- N for $N = 3$ and $N = 4$. The relative performance of all the tested solvers decreases on larger and denser graphs. Intuitively, the size of the MWIS decreases as the graph becomes denser (the average degree increases), hence a wrong selection of a vertex incurs a higher cost in the AR. Also, the MWIS problem is harder on larger graphs due to the larger search space.

Among the centralized solvers, the GCN-based centralized solvers outperform the vanilla CGS on average AR by a gap of 7.7% to 9.2%. The GCN(20)-CRTS achieves the top average AR of 0.989, but is also most sensitive to the graph

²Training typically takes 30 minutes on a workstation with a specification of 16GB memory, 8 cores and Geforce GTX 1070 GPU. The source code is published at <https://github.com/zhongyuanzhao/distgcn>

size (see Fig. 6(b)), since the larger search space lowers its chance of finding a good solution before timeout. Compared to GCN(20)-CRTS, our proposed GCN(1)-CRS-v reduces its runtime by at least two orders of magnitude (i.e., from 5 minutes to up to a few seconds), at the cost of 1.2% average AR, and is less sensitive to graph size. It demonstrates that rollout search can reach a good solution quickly with the same trained model. On the other hand, the performance of rollout search is largely determined by its guiding heuristic. With the guiding heuristic of enhanced CGS described in Section IV-C, the AR of GCN(1)-CRS-e can be boosted by an average of 0.8% from that of GCN(1)-CRS-v. On the ER test set, the GCN(5)-CGS performs similarly as the GCN(1)-CRS-v with slight advantage on denser and larger graphs. It shows that GCN can match the vanilla CGS in estimating the Q values when the test set matches the training set. Moreover, GCN(5)-CGS further reduces the runtime by an order of magnitude on those worst-case instances (i.e., from seconds to sub-seconds)³ and has the lowest sensitivity to graph size.

Our proposed GCN-guided distributed solvers, GCN(1)-LGS and GCN(1)-LGS-it, also outperform the baselines of LGS and MP. Prepending a 1-layer GCN improves LGS by 3.5% on average AR, and this difference is more conspicuous (close to 5%) in the more challenging case of denser graphs. Although MP can find the optimal solution on some sparsely connected graphs (i.e., small average degree), it becomes virtually the same as LGS when the average degree increases to the range of typical conflict graphs in practice (i.e., average degree of 10 to 20). The GCN(1)-LGS-it outperforms GCN(1)-LGS by 0.4% on average, and its advantage is mostly on larger and denser graphs, as feeding the residual graph to GCN(1) improves the consistency. On the other hand, the LGS-3, LGS-4, GCN(1)-LGS-3, and GCN(1)-LGS-4 achieve average ARs of 0.883, 0.896, 0.923, and 0.931, respectively. From the curves of these truncated solvers in Fig. 6, we can find that improperly truncating the LGS can severely degrade the performance on the larger and denser graphs, on which LGS requires more iterations to complete. As shown in [1], increasing the number of layers L from 1 to 3 does not yield better performance.

³For deployment, these presented runtimes can be further optimized.

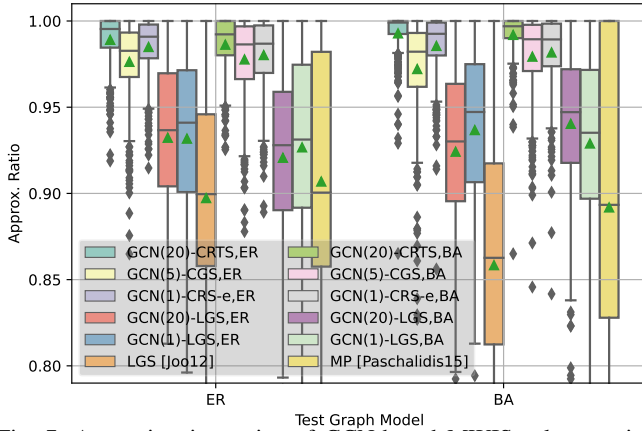


Fig. 7: Approximation ratios of GCN-based MWIS solvers trained on ER and BA models and tested on both settings.

2) *Generalizability*: Next, we examine how well the GCN-based MWIS solvers generalize across graph models. For a given set of hyperparameters, two versions of GCN-based solvers are trained on two different training sets generated from ER and BA models, respectively, with other configurations identical to the default setting. Each version of this solver is then tested on the ER test set of the previous experiment and a BA test set with identical configuration ($m = Vp = \bar{d}$). The ARs of the proposed and baseline solvers on these two test sets are illustrated as mean values in Table III, and as box plots in Fig. 7, where means are marked by green triangles.

Given the heavy-tailed degree distribution of BA graphs [72], the topology-agnostic solvers of LGS and MP experience a drop in performance. In contrast, GCN-based MWIS solvers, regardless of training set, achieve relatively consistent performance on both ER and BA test sets, and outperform LGS and MP by a greater margin in BA graphs, as shown in Table III and Fig. 7, which underscores the value of taking topology into account. In general, GCN-based MWIS solvers tend to perform better if they are trained on the same graph model of the test set, but this influence is small, showing good transferability of the proposed approach. To understand the impact of L , GCNs of 1 layer and 20 layers are evaluated for GCN-LGS. Deeper GCNs do not significantly improve the mean ARs, but tend to present smaller variance compared to shallower GCNs. Moreover, deep GCNs are more tuned to the training graph model. For example, GCN(20)-LGS attains the best performance when trained and tested in BA, but underperforms compared to GCN(1)-LGS when trained on one graph model and tested on the other. A similar pattern can be found in GCN-based centralized solvers, the solver trained and tested on the same graph model has a performance 0.5% greater than when trained and tested on different graph models. Although not shown here, similar transferability holds when varying the vertex utility distribution.

3) *Topology mismatch*: Lastly, we measure the robustness of the reusable topological node embedding \mathbf{z}^G (introduced in Section V-C) against topology changes in wireless networks, which can be attributed to mobility and shadowing. The reusing strategy, denoted as GCN(1:reuse)-LGS, applies the topological embedding $\mathbf{z}^{\mathcal{G}_0}$ generated from a baseline graph \mathcal{G}_0 to 100 instances of similar graphs $\mathcal{G}_i, i \in \{1, \dots, 100\}$

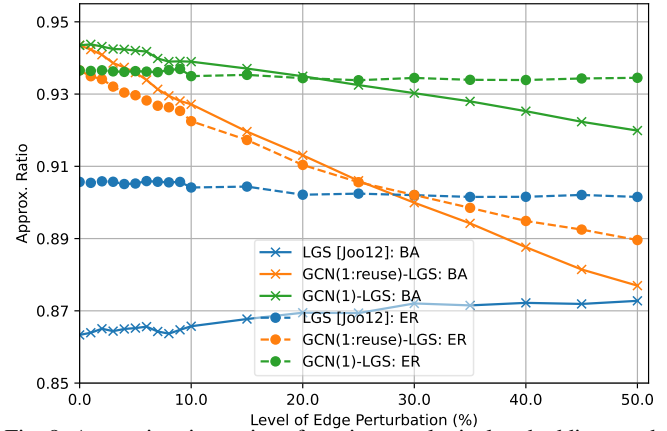


Fig. 8: Approximation ratios of reusing topological embeddings under topology mismatches.

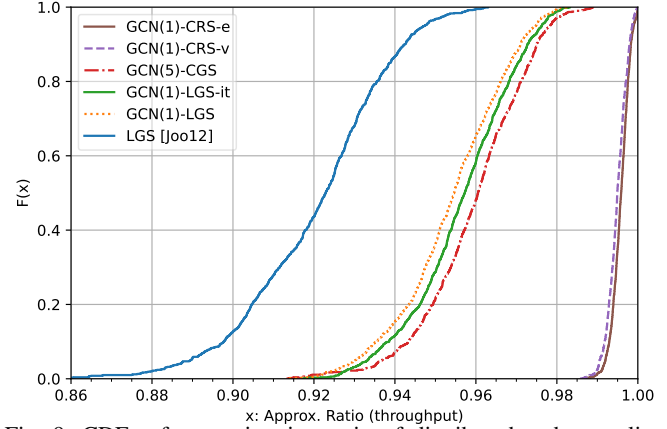


Fig. 9: CDFs of approximation ratio of distributed and centralized throughput-optimal schedulers in oversaturated traffic. The average ARs of these schedulers are listed in Table III.

generated by replacing each edge in \mathcal{G}_0 with a random new edge with a probability equal to the normalized edit distance that measures the level of edge perturbation, and each \mathcal{G}_i is associated with a new realization of random utility $\mathbf{u}_i \sim \mathbb{U}(0, 1)$. The tested baseline graphs are 500 random graphs generated by ER or BA models with $V \in \{100, 150\}$ and $m = \bar{d} \in \{2, 5, 10, 15, 20\}$. The ARs of GCN(1:reuse)-LGS versus the normalized edit distance are illustrated in Fig. 8, along with the LGS and the GCN(1)-LGS using $\mathbf{z}^{\mathcal{G}_i}$ for \mathcal{G}_i , as the control group. On average, the reusable topological embedding $\mathbf{z}^{\mathcal{G}_0}$ can stand up to 30% of edge perturbation on ER graphs and 50% on BA graphs before its gain over LGS diminishes. Note that the control group is also slightly influenced by the topology change, since the underlying degree distribution of the similar graphs generated by our method will shift towards the ER model. Since the topology change of a wireless network is usually several orders of magnitude slower than the channel fading that defines the coherence time slot, this result shows that the reusing strategy detailed in Section V-C allows GCN-LGS to be implemented at the same local complexity of vanilla LGS.

B. GCN-based Throughput-Optimal Scheduling

To understand how the performance of the proposed solvers in synthetic random graphs could be transferred to scheduling, throughput-optimal scheduling in wireless ad-hoc networks

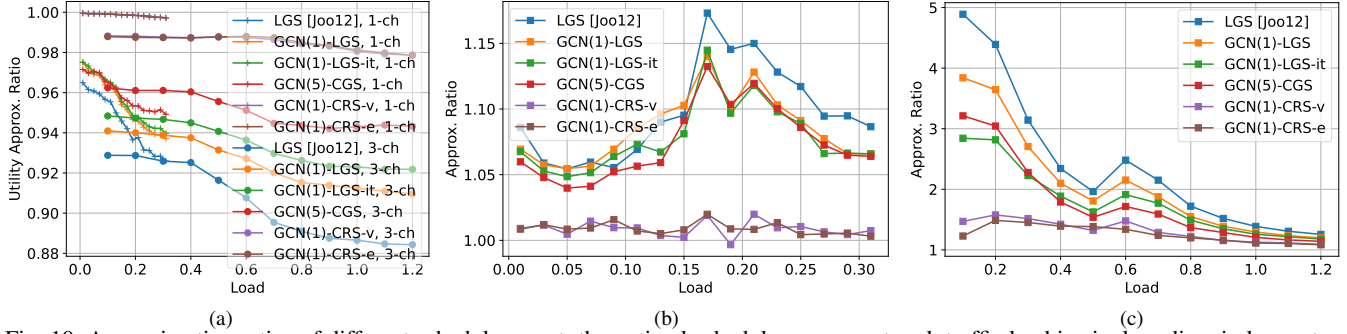


Fig. 10: Approximation ratios of different schedulers w.r.t. the optimal scheduler versus network traffic load in single-radio wireless networks with 1-hop flows and per-link utility $u(v) = q(v)r(v)$. (a) Average total utility achieved per time slot. (b) Median backlog in single-channel scheduling, the saturation load is 0.12. (c) Median backlog in 3-channel scheduling, the saturation load is 0.55.

is simulated. These networks consist of 100 users randomly located in a square of area 250. A link is established if the distance between two users is smaller than 1, and two links interfere with each other if they have incident users within distance of 4. A 1-hop flow with random direction is created on each link. The exogenous packets at each source user node follow a Poisson arrival with a prescribed arrival rate λ . The link rate $r(v)$, defined as the number of packets that can be transmitted through link v in a time slot, is drawn from a normal distribution $\mathcal{N}(50, 25)$ independently across time slots and links, and clipped to $[0, 100]$, to capture a clipped rectified linear function of signal-to-noise ratio (SNR) caused by the effects of fading, constant transmit power, and lognormal shadowing [73]. The network traffic load is defined as $\mu = \mathbb{E}(r)/\lambda$, and is considered as saturated if the average queue length under optimal scheduling equals the average link rate $\mathbb{E}(q|\mu) = \mathbb{E}(r)$. A total of 100 realizations of random wireless networks are generated, typically with 40-60 links, and the average degrees of their conflict graphs range from 7.7 to 26.9 with a mean of 13.2. For each conflict graph, 10 scheduling instances of 200 time slots are executed by each tested scheduler. In each scheduling instance, the same realization of arrivals and link rates is used for each scheduler.

1) *Oversaturated traffic*: We first consider a single-radio single-channel scenario, where the exogenous packets arrive at an oversaturated rate, and the per-link utility is the number of packets the link can deliver, i.e., $u(v) = \min(q(v), r(v))$, where $q(v)$ is the backlog of link v . In this case, the average throughout is identical to the average utility a scheduler achieves per time slot. The average ARs of throughput w.r.t. the optimal scheduler achieved by the tested schedulers are listed in Table III (under the ‘Thpt.’ column). The empirical CDFs of the ARs of these schedulers are illustrated in Fig. 9, which show consistent improvements over LGS from GCN-based schedulers. In oversaturated traffic, the GCN(1)-LGS scheduler closes the suboptimality gap of LGS by 42% on average, while the centralized schedulers GCN(1)-CRS-e and GCN(1)-CRS-v are near optimal.

2) *Varying traffic*: Next, we consider the scenarios of a single-radio wireless network with one and three sub-channels, respectively, in which the traffic load varies from unsaturated to oversaturated regions, and the per link utility function is $u(v) = q(v)r(v)$ [2], [7], [66], [67]. In the second scenario, the multi-channel conflict graph is generated by adding an

edge (v_1^k, v_2^k) for $k \in 1, 2, 3$ at a probability of 90% if edge (v_1, v_2) appears in the single-channel conflict graph of the first scenario. The ARs of achieved utility and median backlog w.r.t. the optimal scheduler are used to evaluate the relative performance of the tested heuristic schedulers versus the traffic load, as presented in Fig. 10.

Across traffic loads and different numbers of sub-channels, the ranking of LGS, GCN(1)-LGS, GCN(1)-LGS-it, GCN(1)-CRS-v, and GCN(1)-CRS-e in relative utility, as illustrated in Fig. 10(a), is consistent with the results on synthetic random graphs and oversaturated traffic. However, compared to single-channel scheduling, all the tested schedulers experience marked drops in relative utility in 3-channel scheduling ($0.1 \leq \mu \leq 0.3$). Since the average degree and size of the 3-channel conflict graph increased by almost three times over the single-channel conflict graph, such drop is consistent with the results in Fig. 6. As the traffic load increases, the relative performance of all the tested heuristics decreases. This is because the accumulation of backlogs raises the floor of per-link utility across the network, the decreased relative variance makes the weights less distinguishable to the heuristics. However, since the utility function $u(v) = q(v)r(v)$ is not designed to optimize the latency, moderate advantages in AR of utility may not always be transferred to latency performance in the stable region, as shown in the relative latency performance of the two scheduling scenarios illustrated in Figs. 10(b) and 10(c), e.g., between GCN(1)-LGS-it and GCN(5)-CGS.

In single-channel scheduling, the saturation traffic load is 0.12, and the ARs of median backlog (the smaller, the better) across traffic loads of the tested schedulers are presented in Fig. 10(b). The centralized schedulers, GCN(1)-CRS-e and GCN(1)-CRS-v (with ARs of 99.5 ~ 100% on utility), can achieve near optimal performance with less than 1% average excessive backlogs. In the unsaturated region ($0.01 \leq \mu \leq 0.12$), the distributed schedulers LGS, GCN(1)-LGS, and GCN(1)-LGS-it, have similar excessive backlogs of 5% to 10%. In the oversaturated region, GCN(1)-LGS and GCN(1)-LGS-it are 2 to 3% better than the LGS. The GCN(1)-LGS-it consistently leads the GCN(1)-LGS by a slight advantage across the traffic load.

In the scenario of 3-channel scheduling, the saturation traffic load is 0.55, the ARs of median backlog across traffic loads achieved by the tested schedulers are presented in Fig. 10(c), of which the rankings are consistent with that of single-channel

scheduling. Due to the increased traffic load and graph size, the median backlog of distributed schedulers is multiple times larger than that of the optimal scheduler in the stable region. The relative performance of the centralized schedulers experiences similar deterioration. The gaps of the relative latency and utility among the heuristic schedulers are also enlarged. These results implicate that one should consider the trade-off between the lowered local complexity (e.g., $\mathcal{O}(K \log V)$ vs. $\mathcal{O}(\log KV)$) and the degraded scheduling performance on larger conflict graphs in specific scenarios when choosing the approach of multi-channel scheduling.

The good performance of GCN(5)-CGS in synthetic random graphs does not transfer to throughput optimal scheduling, in which it only performs slightly better than GCN(1)-LGS-*it*. This result shows that the generalizability of GCN-based deep Q learning across graph types and weight distribution is inferior to the GCN-based rollout search.

C. Concluding Remarks on Numerical Experiments

The numerical results show that a minimal GCN (GCN(1)) with only 2 trainable parameters [cf. (7)], when integrated into various algorithmic frameworks, can substantially close the suboptimality gap of the baseline greedy heuristics for the MWIS problem. The enhancement in an efficient heuristic can be transferred to improved efficiency or performance of more sophisticated exact and approximate solvers, which usually employ efficient heuristics as intermediate steps or to obtain warm-start solutions.

In practice, our centralized solvers require efficient implementations that leverage the sparsity of the graph to realize the computational complexity listed in Tables I. On the other hand, the distributed solver of GCN(1)-LGS can be implemented by increasing the size of control message without additional local exchanges. Lastly, the advantage of GCN-based heuristics over the greedy baseline is more conspicuous for wireless networks that are denser, larger, and with more sub-channels.

VII. CONCLUSIONS AND FUTURE WORK

We presented several graph-aware efficient MWIS solvers for link scheduling in wireless networks. The centralized solver uses a lightweight GCN to guide centralized rollout tree search, and can achieve near optimal performance on small-to middle-sized networks with a complexity of $\mathcal{O}(V^2)$. By leveraging the topology-awareness and distributed nature of GCNs, the distributed solvers enhance the distributed greedy heuristic and retain its efficiency, and can achieve superior performance in larger and denser networks with a local communication complexity of $\mathcal{O}(\log V)$. The GCN can be trained on simulated networks without exactly solving the NP-hard MWIS problem, and generalizes well across different types of graphs. Moreover, our approach is agnostic to the specific per-link utility, thus, it can be used in conjunction with many existing distributed scheduling protocols. Future research efforts include: 1) Incorporating state-awareness into the per-link utility by taking into account the causal relationship between network state transition and scheduling decision, and 2) Considering the scheduling problem for wireless networks operating on non-orthogonal channels.

REFERENCES

- [1] Z. Zhao, G. Verma, C. Rao, A. Swami, and S. Segarra, “Distributed scheduling using graph neural networks,” in *IEEE Int. Conf. on Acoustics, Speech and Signal Process. (ICASSP)*, 2021, pp. 4720–4724.
- [2] L. Tassiulas, “Stability properties of constrained queueing systems and scheduling policies for maximum throughput in multihop radio networks,” *IEEE Trans. on Automatic Control*, vol. 31, no. 12, 1992.
- [3] C. Joo, X. Lin, and N. B. Shroff, “Understanding the capacity region of the greedy maximal scheduling algorithm in multihop wireless networks,” *IEEE/ACM Trans. Netw.*, vol. 17, no. 4, pp. 1132–1145, 2009.
- [4] A. G. Marques, N. Gatsis, and G. B. Giannakis, “Optimal cross-layer design of wireless fading multi-hop networks,” in *Cross Layer Designs in WLAN Systems*, N. Zorba, C. Skianis, and C. Verikoukis, Eds. Leicester, UK: Troubador Pub, 2011.
- [5] A. Kabbani, T. Salonidis, and E. W. Knightly, “Distributed low-complexity maximum-throughput scheduling for wireless backhaul networks,” in *IEEE Intl. Conf. on Computer Comms. (INFOCOM)*, 2007, pp. 2063–2071.
- [6] I. C. Paschalidis, F. Huang, and W. Lai, “A message-passing algorithm for wireless network scheduling,” *IEEE/ACM Trans. Netw.*, vol. 23, no. 5, p. 1528–1541, Oct. 2015.
- [7] X. Lin, N. B. Shroff, and R. Srikant, “A tutorial on cross-layer optimization in wireless networks,” *IEEE J. Sel. Areas Commun.*, vol. 24, no. 8, pp. 1452–1463, 2006.
- [8] S. K. Sarkar, T. G. Basavaraju, and C. Puttamadappa, *Ad hoc mobile wireless networks: principles, protocols and applications* (2nd Ed). CRC Press, 2013.
- [9] J. Kim, G. Caire, and A. F. Molisch, “Quality-aware streaming and scheduling for Device-to-Device video delivery,” *IEEE/ACM Trans. Netw.*, vol. 24, no. 4, p. 2319–2331, Aug. 2016.
- [10] A. Douik, H. Dahrour, T. Y. Al-Naffouri, and M. Alouini, “Distributed hybrid scheduling in multi-cloud networks using conflict graphs,” *IEEE Trans. Commun.*, vol. 66, no. 1, pp. 209–224, 2018.
- [11] M. Gupta, A. Rao, E. Visotsky, A. Ghosh, and J. G. Andrews, “Learning link schedules in self-backhauled millimeter wave cellular networks,” *IEEE Trans. Wireless Commun.*, vol. 19, no. 12, pp. 8024–8038, 2020.
- [12] J. Qiao, L. X. Cai, X. S. Shen, and J. W. Mark, “Enabling multi-hop concurrent transmissions in 60 GHz wireless personal area networks,” *IEEE Trans. Wireless Commun.*, vol. 10, no. 11, pp. 3824–3833, 2011.
- [13] Q. Xia and J. M. Jornet, “Cross-layer analysis of optimal relaying strategies for terahertz-band communication networks,” in *IEEE Intl. Conf. on Wireless and Mobile Computing, Netw. and Comms. (WiMob)*, 2017, pp. 1–8.
- [14] A. Kott, A. Swami, and B. J. West, “The internet of battle things,” *Computer*, vol. 49, no. 12, pp. 70–75, 2016.
- [15] I. F. Akyildiz, A. Kak, and S. Nie, “6G and beyond: The future of wireless communications systems,” *IEEE Access*, vol. 8, pp. 133995–134030, 2020.
- [16] A. Jindal and K. Psounis, “On the efficiency of CSMA-CA scheduling in wireless multihop networks,” *IEEE/ACM Trans. Netw.*, vol. 21, no. 5, pp. 1392–1406, 2013.
- [17] C. Joo and N. B. Shroff, “Local greedy approximation for scheduling in multihop wireless networks,” *IEEE Trans. on Mobile Computing*, vol. 11, no. 3, pp. 414–426, 2012.
- [18] C. Joo, X. Lin, J. Ryu, and N. B. Shroff, “Distributed greedy approximation to maximum weighted independent set for scheduling with fading channels,” *IEEE/ACM Trans. Netw.*, vol. 24, no. 3, pp. 1476–1488, 2015.
- [19] S. Sanghavi, D. Shah, and A. S. Willsky, “Message passing for maximum weight independent set,” *IEEE Trans. Info. Theory*, vol. 55, no. 11, pp. 4822–4834, 2009.
- [20] P. Du and Y. Zhang, “A new distributed approximation algorithm for the maximum weight independent set problem,” *Mathematical Problems in Engineering*, vol. 2016, 2016.
- [21] X. Li, P. Tolmachev, M. Pauley, and J. H. Manton, “A distributed transmission scheduling algorithm for wireless networks based on the ising model,” in *IEEE Statistical Signal Processing Workshop (SSP)*, 2018, pp. 6–10.
- [22] C. Joo, G. Sharma, N. B. Shroff, and R. R. Mazumdar, “On the complexity of scheduling in wireless networks,” *EURASIP Journal on Wireless Commun. and Netw.*, vol. 2010, no. 1, p. 418934, 2010.
- [23] W. Cheng, X. Cheng, T. Znati, X. Lu, and Z. Lu, “The complexity of channel scheduling in multi-radio multi-channel wireless networks,” in *IEEE Intl. Conf. on Computer Comms. (INFOCOM)*, 2009, pp. 1512–1520.

[24] I. Kadota, A. Sinha, E. Uysal-Biyikoglu, R. Singh, and E. Modiano, “Scheduling policies for minimizing age of information in broadcast wireless networks,” *IEEE/ACM Trans. Netw.*, vol. 26, no. 6, pp. 2637–2650, 2018.

[25] D. Xue, “Delay-oriented analysis and design of optimal scheduling algorithms,” Ph.D. dissertation, Dept. Electrical and Computer Engineering, The Ohio State University, 2013.

[26] W. Ogryczak, H. Luss, M. Pióro, D. Nace, and A. Tomaszewski, “Fair optimization and networks: A survey,” *Journal of Applied Mathematics*, vol. 2014, 2014.

[27] A. Lucas, “Ising formulations of many NP problems,” *Frontiers in Physics*, vol. 2, p. 5, 2014.

[28] W. Lee, M. Kim, and D. Cho, “Deep power control: Transmit power control scheme based on convolutional neural network,” *IEEE Commun. Lett.*, vol. 22, no. 6, pp. 1276–1279, 2018.

[29] S. Wang, H. Liu, P. H. Gomes, and B. Krishnamachari, “Deep reinforcement learning for dynamic multichannel access in wireless networks,” *IEEE Trans. Cognitive Comm. and Netw.*, vol. 4, no. 2, pp. 257–265, 2018.

[30] Y. S. Nasir and D. Guo, “Multi-agent deep reinforcement learning for dynamic power allocation in wireless networks,” *IEEE J. Sel. Areas Commun.*, vol. 37, no. 10, pp. 2239–2250, 2019.

[31] C. Zhang, P. Patras, and H. Haddadi, “Deep learning in mobile and wireless networking: A survey,” *IEEE Commun. Surveys & Tutorials*, vol. 21, no. 3, pp. 2224–2287, 2019.

[32] Z. Qin, H. Ye, G. Y. Li, and B. F. Juang, “Deep learning in physical layer communications,” *IEEE Wireless Commun.*, vol. 26, no. 2, pp. 93–99, 2019.

[33] A. Chowdhury, G. Verma, C. Rao, A. Swami, and S. Segarra, “Unfolding wmmse using graph neural networks for efficient power allocation,” *IEEE Trans. Wireless Commun.*, pp. 1–1, 2021.

[34] A. Kumar, G. Verma, C. Rao, A. Swami, and S. Segarra, “Adaptive contention window design using deep Q-learning,” in *IEEE Int. Conf. on Acoustics, Speech and Signal Process. (ICASSP)*, 2021, pp. 4950–4954.

[35] D. Xu, X. Chen, C. Wu, S. Zhang, S. Xu, and S. Cao, “Energy-efficient subchannel and power allocation for hetnets based on convolutional neural network,” in *IEEE Veh. Technol. Conf. (VTC)*, 2019, pp. 1–5.

[36] T. Van Chien, E. Björnson, and E. G. Larsson, “Sum spectral efficiency maximization in massive MIMO systems: Benefits from deep learning,” in *IEEE Intl. Conf. on Commun. (ICC)*, 2019, pp. 1–6.

[37] W. Cui, K. Shen, and W. Yu, “Spatial deep learning for wireless scheduling,” *IEEE J. Sel. Areas Commun.*, vol. 37, no. 6, pp. 1248–1261, 2019.

[38] M. Eisen and A. R. Ribeiro, “Optimal wireless resource allocation with random edge graph neural networks,” *IEEE Trans. Signal Process.*, 2020.

[39] T. N. Kipf and M. Welling, “Semi-supervised classification with graph convolutional networks,” in *Intl. Conf. Learn. Repres. (ICLR)*, Toulon, France, April 2017.

[40] F. Gama, A. G. Marques, G. Leus, and A. Ribeiro, “Convolutional neural network architectures for signals supported on graphs,” *IEEE Trans. Signal Process.*, vol. 67, no. 4, pp. 1034–1049, 2018.

[41] T. M. Roddenberry and S. Segarra, “HodgeNet: Graph neural networks for edge data,” in *Asilomar Conf. Signals, Systems, and Computers*, 2019, pp. 220–224.

[42] J. Yang and S. Segarra, “Enhancing geometric deep learning via graph filter deconvolution,” in *IEEE Global Conf. Signal and Info. Process. (GlobalSIP)*, Nov 2018, pp. 758–762.

[43] E. Khalil, H. Dai, Y. Zhang, B. Dilks, and L. Song, “Learning combinatorial optimization algorithms over graphs,” in *Advances in Neural Info. Process. Systems*, 2017, pp. 6348–6358.

[44] Z. Li, Q. Chen, and V. Koltun, “Combinatorial optimization with graph convolutional networks and guided tree search,” in *Advances in Neural Info. Process. Systems*, 2018, pp. 539–548.

[45] F. Scarselli, M. Gori, A. C. Tsoi, M. Hagenbuchner, and G. Monfardini, “The graph neural network model,” *IEEE Trans. on Neural Networks*, vol. 20, no. 1, pp. 61–80, 2008.

[46] P. W. Battaglia *et al.*, “Relational inductive biases, deep learning, and graph networks,” *arXiv preprint arXiv:1806.01261*, 2018.

[47] Z. Wu, S. Pan, F. Chen, G. Long, C. Zhang, and S. Y. Philip, “A comprehensive survey on graph neural networks,” *IEEE Trans. on Neural Networks and Learning Systems*, 2020.

[48] J. T. Linderoth and M. W. Savelsbergh, “A computational study of search strategies for mixed integer programming,” *INFORMS Journal on Computing*, vol. 11, no. 2, pp. 173–187, 1999.

[49] G. J. Woeginger, “Exact algorithms for NP-hard problems: A survey,” in *Combinatorial optimization—eureka, you shrink!*, M. Jünger, G. Reinelt, and G. Rinaldi, Eds. Berlin, Germany: Springer, 2003, pp. 185–207.

[50] J. S. Warren and I. V. Hicks, “Combinatorial branch-and-bound for the maximum weight independent set problem,” *Relatório Técnico, Texas A&M University, Citeseer*, vol. 9, p. 17, 2006.

[51] J. Puchinger and G. R. Raidl, “Combining metaheuristics and exact algorithms in combinatorial optimization: A survey and classification,” in *International work-conference on the interplay between natural and artificial computation*. Springer, 2005, pp. 41–53.

[52] K. Verhetsel, “Solving the maximum weight independent set problem: application to indirect hex-mesh generation,” Master’s thesis, Ecole polytechnique de Louvain, Université catholique de Louvain, 2017.

[53] S. Lamm, C. Schulz, D. Strash, R. Williger, and H. Zhang, “Exactly solving the maximum weight independent set problem on large real-world graphs,” in *Proc. of the 21st Workshop on Algorithm Engineering and Experiments (ALENEX)*. SIAM, 2019, pp. 144–158.

[54] G. O. LLC, “Gurobi optimizer reference manual,” 2020. [Online]. Available: <http://www.gurobi.com>

[55] W. Pullan, “Phased local search for the maximum clique problem,” *Journal of Combinatorial Optimization*, vol. 12, no. 3, pp. 303–323, 2006.

[56] ———, “Optimisation of unweighted/weighted maximum independent sets and minimum vertex covers,” *Discrete Optimization*, vol. 6, no. 2, pp. 214–219, 2009.

[57] Q. Wu, J.-K. Hao, and F. Glover, “Multi-neighborhood tabu search for the maximum weight clique problem,” *Annals of Operations Research*, vol. 196, no. 1, pp. 611–634, 2012.

[58] U. Benlic and J.-K. Hao, “Breakout local search for the quadratic assignment problem,” *Applied Mathematics and Computation*, vol. 219, no. 9, pp. 4800–4815, 2013.

[59] J. Choi, S. Oh, and J. Kim, “Energy-efficient cluster head selection via quantum approximate optimization,” *Electronics*, vol. 9, no. 10, p. 1669, 2020.

[60] T. Ameen ur Rahman, M. S. Hassan, and M. H. Ismail, “A queue-length based approach to metropolized hamiltonians for distributed scheduling in wireless networks,” in *Wireless Telecom. Symp. (WTS)*, 2020, pp. 1–6.

[61] A. Mittal, A. Dhawan, S. Manchanda, S. Medya, S. Ranu, and A. Singh, “Learning heuristics over large graphs via deep reinforcement learning,” *arXiv preprint arXiv:1903.03332*, 2019.

[62] D. Selsam, M. Lamm, B. Bünz, P. Liang, L. de Moura, and D. L. Dill, “Learning a SAT solver from single-bit supervision,” in *Intl. Conf. Learn. Repres. (ICLR)*, 2019.

[63] M. Prates, P. H. Avelar, H. Lemos, L. C. Lamb, and M. Y. Vardi, “Learning to solve NP-complete problems: A graph neural network for decision TSP,” in *Proceedings of the AAAI Conference on Artificial Intelligence*, vol. 33, 2019, pp. 4731–4738.

[64] J. M. Tönshoff, M. Ritzert, H. Wolf, and M. Grohe, “Graph neural networks for maximum constraint satisfaction,” *Frontiers in Artificial Intelligence*, vol. 3, p. 98, 2020.

[65] J. Yang, S. C. Draper, and R. Nowak, “Learning the interference graph of a wireless network,” *IEEE Trans. Signal Inf. Process. Netw.*, vol. 3, no. 3, pp. 631–646, 2016.

[66] X. Lin and S. Rasool, “A distributed joint channel-assignment, scheduling and routing algorithm for multi-channel ad-hoc wireless networks,” in *IEEE Intl. Conf. on Computer Comms. (INFOCOM)*, 2007, pp. 1118–1126.

[67] V. Bhandari and N. H. Vaidya, “Scheduling in multi-channel wireless networks,” in *Intl. Conf. on Distributed Computing and Networking (ICDCN)*. Springer, 2010, pp. 6–17.

[68] D. Bertsekas, “Rollout, policy iteration, and distributed reinforcement learning,” *Athena Scientific*, vol. 1, 2020.

[69] A. Kako, T. Ono, T. Hirata, and M. M. Halldórsson, “Approximation algorithms for the weighted independent set problem in sparse graphs,” *Discrete Applied Mathematics*, vol. 157, no. 4, pp. 617–626, 2009.

[70] Z. Zhao, G. Verma, C. Rao, A. Swami, and S. Segarra, “Supplemental materials for link scheduling using graph neural networks,” 2021.

[71] P. Erdős and A. Rényi, “On random graphs I,” *Publ. Math. Debrecen* 6, pp. 290–297, 1959.

[72] R. Albert and A.-L. Barabási, “Statistical mechanics of complex networks,” *Rev. Mod. Phys.*, vol. 74, pp. 47–97, Jan 2002. [Online]. Available: <https://link.aps.org/doi/10.1103/RevModPhys.74.47>

[73] H. Mousavi, I. S. Amiri, M. Mostafavi, and C. Choon, “LTE physical layer: Performance analysis and evaluation,” *Applied Computing and Informatics*, vol. 15, no. 1, pp. 34 – 44, 2019.

Supplemental Materials for Link Scheduling using Graph Neural Networks

Zhongyuan Zhao, Gunjan Verma, Chirag Rao, Ananthram Swami, and Santiago Segarra

arXiv:2109.05536v1 [eess.SP] 12 Sep 2021

I. GCN-GUIDED CENTRALIZED RANDOM TREE SEARCH

The GCN-guided centralized random tree search (*GCN-CRTS*) is modified from a similar solver of the unweighted MIS problem [1]. The basic idea of GCN-CRTS is to reach as many random terminal nodes as possible in a given time interval to increase its chance of finding a good solution from them.

A. Iterative Framework

Compared to GCN-CRS in the main manuscript [2], the GCN-CRTS has a similar iterative algorithmic framework, as illustrated in Fig. 1, and the same definition of search tree. The possible transitions of the state of each iteration form a search tree, as illustrated in Fig 1(b). The solver finds an approximate solution by traversing from the root of the search tree to a terminal state.

On initialization, the root node is pushed into the search queue. In each iteration, the solver expands a non-terminal node and proceeds to a child node in 7 steps, as illustrated in Fig. 1(a). In step 1, a non-terminal node $\langle \mathcal{G}', \mathbf{u}', \mathbf{v}', \mathcal{N}(\mathbf{v}') \rangle$ is randomly popped from the search queue, of which the enclosed residual graph \mathcal{G}' and residual utility vector \mathbf{u}' are fed into the GCN. In step 2, based on the inputs of \mathcal{G}' and \mathbf{u}' , the GCN generates the node embedding matrix $\mathbf{Z}' \in \mathbb{R}^{V' \times B}$, which collects the topology-aware scaling factor $\mathbf{Z}'_{v,b} = z'_b(v)$ for all $v \in \mathcal{V}'$ and $b \in \{1, \dots, B\}$, as $\mathbf{Z}' = \Psi_{\mathcal{G}'}(\mathbf{u}'; \Xi)$, where B is the branching factor of the search tree configured to create a large search tree with a large amount of distinct terminal nodes, $\Psi_{\mathcal{G}'}$ is an L -layered GCN defined on the graph \mathcal{G}' , \mathbf{u}' is the residual utility vector, and Ξ represents the collection of trainable parameters of the GCN. In step 3, a prediction matrix $\mathbf{W}' \in \mathbb{R}^{V' \times B}$ is created from \mathbf{Z}' and \mathbf{u}' , of which an element $\mathbf{W}'_{v,b} = w'_b(v) = z'_b(v) \cdot u'(v)$ represents the topology-aware utility of vertex v . In step 4, each column of the prediction matrix is sorted in descending order. More precisely, denoting by $\mathbf{X}_{*,i}$ the i th column of the generic matrix \mathbf{X} , we obtain

Z. Zhao and S. Segarra are with the Department of Electrical and Computer Engineering, Rice University, USA. e-mails: {zhongyuan.zhao, segarra}@rice.edu

G. Verma, C. Rao, and A. Swami are with the US Army's DEVCOM Army Research Laboratory, USA. e-mails: {gunjan.verma.civ, chirag.r.rao.civ, ananthram.swami.civ}@mail.mil.

Research was sponsored by the Army Research Office and was accomplished under Cooperative Agreement Number W911NF-19-2-0269. The views and conclusions contained in this document are those of the authors and should not be interpreted as representing the official policies, either expressed or implied, of the Army Research Office or the U.S. Government. The U.S. Government is authorized to reproduce and distribute reprints for Government purposes notwithstanding any copyright notation herein.

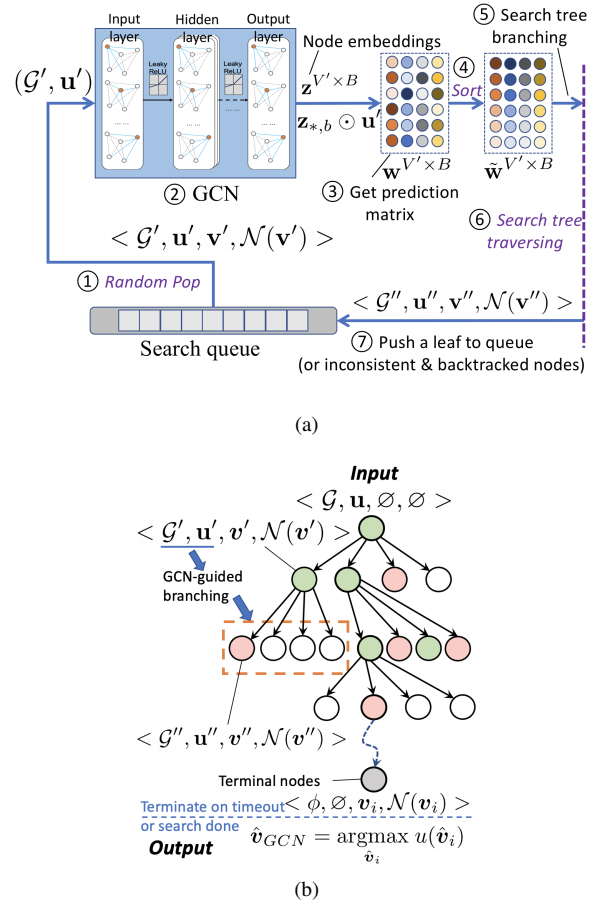


Fig. 1: Architecture of GCN-based centralized MWIS solvers. (a) Iterative framework of GCN-guided tree search. (b) Random tree search with timeout, where the consistent and inconsistent nodes are marked by green and red, respectively.

the sorted prediction matrix $\tilde{\mathbf{W}}'_{*,b} = \text{sort}(\mathbf{W}'_{*,b})$ and the sorted vertex matrix $\tilde{\mathbf{V}}'_{*,b} = \text{argsort}(\mathbf{W}'_{*,b})$, as illustrated in Fig. 1(a) where elements in \mathbf{W}' and $\tilde{\mathbf{W}}'$ with larger values are represented by darker colors. Next, in step 5, up to B prediction vertices are extracted from the sorted vertex matrix $\tilde{\mathbf{V}}'$ to create the B branches (next states) of the current node (current state) in the search tree, respectively. The child node $\langle \mathcal{G}'', \mathbf{u}'', \mathbf{v}'', \mathcal{N}(\mathbf{v}'') \rangle$ on a branch is generated based on one of the B prediction vertices, denoted as v , as follows:

$$\mathcal{G}'' = \mathcal{G}' \setminus (v \cup \mathcal{N}(v)), \mathbf{v}'' = \mathbf{v}' \cup \{v\}. \quad (1)$$

In step 6, the solver selects one of the B children nodes to proceed according to the traversing strategy detailed in Sections I-C. Lastly, in step 7, if the selected child node (next

state) is a non-terminal node, it is pushed into the search queue as a new leaf in the search tree.

B. Graph Convolutional Network Design

The GCN in GCN-CRTS has the same input and hidden layers as the GCN in the main manuscript [2], and a slightly different output structure. The output layer of GCN has a dimension of $g_L = 2B$, with sigmoid/softmax activation applied to B pairs of logits. In each pair of logits for vertex v , the first element is the probability that $v \in \mathbf{v}^*$ and the second element is probability that $v \notin \mathbf{v}^*$, where \mathbf{v}^* is an MWIS for input $(\mathcal{G}', \mathbf{u}')$. The node embedding matrix $\mathbf{Z}' \in [0, 1]^{V' \times B}$ is obtained by extracting the first elements of the B pairs of logits for all $v \in \mathcal{V}'$. The GCN is trained by supervised learning, as detailed in Section I-C.

C. Random Tree Search

At step 6 of each algorithmic iteration described in Section I-A, the GCN-CRTS traverses the search tree as follows: First, a column $b \in \{1, \dots, B\}$ of the sorted vertex matrix $\tilde{\mathbf{V}'}$ is selected uniformly at random. Then, a depth first search is performed by testing the vertices in $\tilde{\mathbf{V}}'_{*,b}$ one by one according to (1), until reaching a terminal node (gray node in Fig. 1(b)) or an inconsistent node (pink nodes in Fig. 1(b)). If the tested vertex $v \in \mathcal{N}(\mathbf{v}'')$, the node $\langle \mathcal{G}'', \mathbf{u}'', \mathbf{v}'', \mathcal{N}(\mathbf{v}'') \rangle$ is marked as inconsistent and pushed to the search queue in Fig. 1. To ensure that all terminal nodes could be reached, a backtracking mechanism is employed so that each consistent node can also be pushed to the search queue with some prescribed probability. The search is terminated on timeout or the condition of all terminal nodes being reached, and the output is the best solution observed throughout the tree search

$$\hat{\mathbf{v}}_{GCN} = \underset{\hat{\mathbf{v}}_i}{\operatorname{argmax}} u(\hat{\mathbf{v}}_i), \quad (2)$$

where $\hat{\mathbf{v}}_i$ is the solution from the i th terminal node being reached. To improve the quality of the solution, the search tree can be traversed by multiple parallel threads that share the same search queue to reach more terminal nodes before timeout.

D. Training

The GCN in GCN-CRTS is trained by supervised learning with a loss function [1]

$$\ell(\mathbf{\Xi}; \mathcal{G}, \mathbf{u}, \mathbf{y}) = \min_{b=1}^B \frac{1}{V} \sum_{v=1}^V \mathcal{C}(\mathbf{y}_v, \mathbf{Z}_{v,b}), \quad (3)$$

where $\mathbf{y} \in \{0, 1\}^V$ is the label vector ($\mathbf{y}_v = 1$ if $v \in \mathbf{v}^*$ and 0 otherwise) and $\mathcal{C}(y, z) = -[y \log(z) + (1 - y) \log(1 - z)]$ is the cross entropy function. Synthetic random graphs are used as the training data. Since obtaining the optimal solution is NP-hard, the label vector \mathbf{y} is generated by heuristics for computational efficiency. Specifically, the labels are generated by selecting the best solution from two guiding heuristics: linear programming [3] and centralized greedy solver. Thanks to the iterative framework and nature of GCN, the GCN-CRTS

can generalize and outperform the training graphs and labels in terms of size [1] and quality. However, the GCN-CRTS will take a relatively long time to find a good solution (e.g., several minutes), therefore is not suitable for link scheduling.

II. GCN-GUIDED CENTRALIZED GREEDY SEARCH

Compared to GCN-CRTS, GCN-guided centralized greedy search (*GCN-CGS*) can reach a good terminal node quickly, thus suitable for link scheduling. The GCN-CGS is modified from the deep Q network in [4] by replacing the Node2Vec module with a GCN, with implementation detailed as follows.

The iterative framework of GCN-CGS is almost identical to that of GCN-CRS with only two exceptions: 1) The branching factor $B = |\mathcal{V}'|$ is no longer a hyperparameter. 2) Instead of \mathbf{w}' , the node embedding $\mathbf{z}' \in \mathbb{R}^{V'}$ is directly used as the vector of Q values of the action space. For a non-terminal node $\langle \mathcal{G}', \mathbf{u}', \mathbf{v}', \mathcal{N}(\mathbf{v}') \rangle$ in the search tree, the observation of the agent is $x' = (\mathcal{G}', \mathbf{u}')$, where \mathcal{G}' is the residual graph, \mathbf{u}' is the corresponding utility vector, and the action space \mathcal{A}' of the agent is the vertex set \mathcal{V}' of the graph \mathcal{G}' . With the input $(\mathcal{G}', \mathbf{u}')$, the GCN generates the node embedding \mathbf{z}' as the Q values of the action space, based on which the action is selected by an ϵ -greedy policy. The next state $x'' = (\mathcal{G}'', \mathbf{u}'')$ is generated according to (1). The search terminates upon reaching a terminal node.

The GCN is trained by finite-horizon reinforcement learning with a discount rate of 1.0. The reward is defined as $\gamma = 0$ for a non-terminal state, and $\gamma = u(\hat{\mathbf{v}}_{GCN})/u(\hat{\mathbf{v}}_{Gr})$ for a terminal state, where $\hat{\mathbf{v}}_{Gr}$ is obtained by the vanilla centralized greedy solver. In each iteration, the tuple of $\langle x', \mathcal{A}', \gamma, x'', done \rangle$ is saved to the replay buffer of the agent, where *done* is a boolean variable indicating if x' is on a terminal node. The GCN is trained by standard experience replay as used in deep Q learning. The exploration rate ϵ is initialized to 1 and decays exponentially during training, and set to 0 for testing and deployment. The GCN-CGS is enabled by the fact that a GCN can have state and action space of any dimensions.

REFERENCES

- [1] Z. Li, Q. Chen, and V. Koltun, “Combinatorial optimization with graph convolutional networks and guided tree search,” in *Advances in Neural Info. Process. Systems*, 2018, pp. 539–548.
- [2] Z. Zhao, G. Verma, C. Rao, A. Swami, and S. Segarra, “Link scheduling using graph neural networks,” in *submitted to IEEE J. Sel. Topics Signal Process.*, 2021.
- [3] A. Kako, T. Ono, T. Hirata, and M. M. Halldórsson, “Approximation algorithms for the weighted independent set problem in sparse graphs,” *Discrete Applied Mathematics*, vol. 157, no. 4, pp. 617–626, 2009.
- [4] E. Khalil, H. Dai, Y. Zhang, B. Dilkina, and L. Song, “Learning combinatorial optimization algorithms over graphs,” in *Advances in Neural Info. Process. Systems*, 2017, pp. 6348–6358.